International Journal of Solids and Structures 51 (2014) 1003–1019

Contents lists available at ScienceDirect

International Journal of Solids and Structures

journal homepage: www.elsevier.com/locate/ijsolstr

Poynting and axial force–twist effects in nonlinear elastic mono- and bi-layered cylinders: Torsion, axial and combined loadings

Dong Wang, M.S. Wu *

School of Mechanical and Aerospace Engineering, Nanyang Technological University, 50 Nanyang Avenue, Singapore 639798, Singapore

ARTICLE INFO

Article history:
Received 15 July 2013
Received in revised form 21 November 2013
Available online 6 December 2013

Keywords:
Poynting effect
Coupled axial force–twist effect
Bilayers
Torsion-axial loading
Second-order elasticity

ABSTRACT

The Poynting effect, in which a cylinder elongates or contracts axially under torsion, is an important nonlinear phenomenon in soft materials. In this paper, analytical solutions are obtained for homogeneous and bi-layered cylinders under torsion, axial and combined loadings, employing second-order elasticity and Lagrangian equilibrium equations. Explicit parameters for judging the sign of the Poynting effect are given. It is found that the effect in a soft composite may be significantly amplified over that in homogeneous materials and that it is strongly influenced by the interface position and by the material configuration in the composite. A coupled axial force–twist effect under combined loading, i.e., the twist of a torsionally loaded cylinder can be affected by the axial loading, is also found. Comparison of the predictions with the torque-tension-twist data for cardiac papillary muscles shows reasonable agreement. The solutions also provide the basis for a mechanistic method of determining third-order elastic constants.

1. Introduction

Soft materials such as synthetic polymers have a very diverse range of applications, e.g., drug delivery (Brazel and Peppas, 1999), tissue scaffolding (Stammen et al., 2001), miniature sensors (Han et al., 2002) and actuators (Beebe et al., 2000). The mechanical properties of biopolymer networks also play an essential role in many physiological functions of cells and tissues (Janmey et al., 2007). A common feature of soft materials is their nonlinearity, which distinguishes them from materials such as ceramics and metals. The Poynting effect, i.e., a cylindrical specimen elongates or contracts in the axial direction under torsion, is one of the important nonlinear phenomena. It has long been recognized that many elastic materials exhibit the positive Poynting effect when subjected to torsion (Poynting, 1909; Rivlin, 1953). However, recent discovery shows that many biopolymers exhibit the negative Poynting effect under torsion or shear. Networks of semiflexible biopolymers (actin, vimentin, neurofilaments) may generate negative normal stresses of magnitude comparable to the applied shear stress (Janmey et al., 2007; Kang et al., 2009; Conti and MacKintosh, 2009), or equivalently, they contract axially under torsion.

A number of models have been used to investigate the Poynting effect, as briefly reviewed below. Mihai and Goriely (2011) imposed a set of adscititious inequalities related to material parameters for describing the Poynting effect of hyperelastic materials subjected to simple or pure shear. Both the positive and negative effects are possible according to these inequalities. In a later paper, they also studied the Poynting effect via the finite element method (Mihai and Goriely, 2013). In this work, they emphasized that for a small triaxial stretch superimposed on simple shear, the normal stress contribution due to the triaxial stretch should be removed to judge if the Poynting effect exists. Similarly, when *pure* shear is imposed on an axially stretched solid, the Poynting effect should be defined with respect to the length after pre-stretching and not the initial length before any loading is imposed. Horgan and Murphy (2011), employing a logarithmic form for the strain energy densities of incompressible anisotropic materials, showed that the negative Poynting effect is generated in the presence of large material anisotropy and is also present under certain loading conditions. Misra et al. (2010) experimentally showed that the negative normal stress in anisotropic myocardial tissue under shear is larger than in Sylgard gel, which they also described theoretically using an exponential form and an Ogden form of the strain energy densities for the tissue and the gel, respectively. Wu and Kirchner (2010) showed that the negative Poynting effect is generally possible for biogels. Their work is based on second-order elasticity. Kang et al. (2009) developed microstructural models which

* Corresponding author. Tel.: +65 6790 5545.
E-mail address: mmswu@ntu.edu.sg (M.S. Wu).

0020-7683/$ - see front matter © 2013 Elsevier Ltd. All rights reserved.
http://dx.doi.org/10.1016/j.ijsolstr.2013.11.027

consider filament bending and tension energies as well as thermal fluctuations. These are used to predict the direction and magnitude of the normal stress under shear. Janmey et al. (2007) developed a microstructural model, based on the transition from a bending-dominated to a stretching-dominated phase of the filaments, in order to interpret the negative normal stress effect. Zubov (2001) developed an expression to determine the Poynting effect in isotropic incompressible materials, for which an explicit expression was given for a neo-Hookean material. Earlier works on second-order torsion such as those of Bhargava and Gupta (1976, 1979) and Blackburn and Green (1957) did not study the Poynting effect or the problem of combined torsion-axial loading. Green and Shield (1951) examined the problem of a small twist superposed on finite extension, and again the Poynting effect was not the objective of their investigation.

To our knowledge, the problem of the Poynting effect in multilayered composites has received little attention. On the other hand, many natural biomaterials such as skin, heart valves, articular cartilage, small-intestinal submucosa and vascular tissues are multilayered, see for example Diridollou et al. (2000), Sofer et al. (2002), Alexopoulos et al. (2003), Stella and Sacks (2007), Zhao et al. (2011) and Browning et al. (2012). Criscione et al. (1999) investigated the twist rate of cardiac capillary muscles under a constant axial stretch as a function of the twisting moment. The muscles are considered as composites consisting of a core of myocardium inside a thin sheath of endocardium. Another example is the stroma of the cornea, made up of collagen fibrils embedded in a hydrated matrix of proteoglycans, glycoproteins and keratocytes. The biomechanical response plays a critical part in corrective surgeries such as LASIK and diseases such as keratoconus and corneal dystrophies (Boyce et al., 2007). In general, connective tissues such as tendons and ligaments are fiber-reinforced soft composite materials, and the issues of nonlinearity, finite strains, anisotropy and viscoelasticity have been active areas of research (Limbert and Taylor, 2002). Furthermore, multilayered hydrogel networks can also be synthesized (Cuchiara et al., 2010) for many applications such as tissue regeneration, wound healing and drug delivery (Detzel et al., 2011; Jessel et al., 2006). Zhu et al. (2004) used a polyelectrolyte multilayer technique to create multilayer coating on poly-(DL-lactide) to promote chondrocyte attachment and growth. A layer-by-layer technique was also used to create multilayer coatings of chitosan and heparin on biomaterials to control MG-63 osteoblast adhesion and growth (Kirchhof et al., 2009). A multilayer biomimetic scaffold mimicking the structure of cancellous and cortical bones was designed for bone tissue engineering, which shows an enhanced mechanical strength and larger pore size in the center (Kong et al., 2007). In a physiological environment, biomaterials are often subjected to complex loading which may involve torsion and axial loading (tension or compression). The combined torsion-tension loading of a multilayered cylinder is thus of major interest.

In this paper, the analytical solutions for cylindrical multilayered composites under pure torsion, pure axial loading and combined torsion-axial loading are obtained within the framework of Murnaghan's (1951) second-order elasticity theory. The focus of the work is on the Poynting effect in soft and metallic composites. A further interesting question is, in contrast to the Poynting effect described thus far, whether an axial loading can contribute to the twist of the cylinder. We shall call this the "axial force–twist effect." The Poynting effect refers to the axial deformation of a cylinder under pure torsion, and was named in honor of Poynting (1909). This effect can be positive or negative. The axial force–twist effect can also be positive or negative, the former meaning that both the torsion and axial loadings produce twist in the same sense while the latter meaning that they produce twist in mutually opposite sense. We further note that under pure axial loading of a circular cylinder, the twist or rotational displacement is necessarily zero because of the axisymmetric constraint. This means that the Poisson effect for this displacement component does not exist in the usual sense. The Poisson effect exists for the radial displacement under pure axial loading. Hence, the axial force–twist effect, which is judged by the rotational displacement, is not associated with the Poisson effect. The axial force–twist effect is rarely discussed in the literature, an exception being Zubov (2001), who investigated it in terms of an isotropic incompressible neo-Hookean material. The term "inverse Poynting effect" was used by Zubov (2001), but it should not be confused with the term "negative Poynting effect".

The contributions of the current work can be summarized as follows: (1) consideration of bi-layered composites under torsion, axial and combined loadings, (2) elucidation of the second-order effects on mechanical behavior, (3) identification of the coupled components of the elastic fields under combined loading, (4) development of an explicit material- and geometry-dependent parameter for predicting the Poynting effect, (5) investigation of how material properties and geometrical configurations can influence the nonlinear phenomena, thus opening the possibility of designing bio-inspired multilayered composites with desirable characteristics, (6) exploration of the axial force–twist effect, and (7) determination of the third-order elastic constants of soft materials through the Poynting effect dependence on the radii of the constituent layers.

The paper is organized in following manner. In Section 2, the second-order nonlinear elastic model is established and analytical solutions are obtained for bi-layered cylinders under torsion, axial and combined loadings and specialized for (monolayered) homogeneous cylinders. In Section 3, the effects of material nonlinearity and geometrical complexities are presented, highlighting nonlinear phenomena such as the Poynting effect and the axial force–twist effect, as well as the existence of second-order normal stresses. Further discussions, especially for applications of results, are given in Section 4. A summary of the present work is given in Section 5.

2. Formulation and solutions

Consider an N-layered circular cylinder of length L and radius r_N (or simply R for a homogeneous cylinder). The interfaces are located at the radial coordinates $r = r_i$, $i = 1, N-1$, with $i = 1$ denoting the innermost interface, as shown in Fig. 1. All the layers are nonlinear elastic, isotropic, homogeneous and perfectly bonded to each other. The composite cylinder is subjected to either a torsion T, an axial loading P (tension or compression), or a combined T–P, with respect to the longitudinal direction. The initial coordinates of a particle of the cylinder are chosen as (r,θ,z), which respectively represent the radial, angular and axial coordinates. The final coordinates are denoted by (ρ,ψ,ζ).

Murnaghan (1951) has investigated the pure torsion, and partially the pure tensile loading, of a homogeneous cylinder. Besides the second-order elasticity framework of Murnaghan, one may adopt various forms of the strain energy density functions, e.g., neo-Hookean, Mooney-Rivlin, St. Venant–Kirchhoff, Ogden, and polynomial forms. The Murnaghan energy density function is chosen for the following reasons: (1) it is general rather than specific and the linear and second-order nonlinear effects can be distinguished; (2) the elastic properties are captured by two second-order and three third-order elastic constants, which can be determined through measuring speed variations of shear waves as a function of applied stress (Catheline et al., 2003); (3) analytical solutions can be obtained for multilayered geometries as found in this work; and (4) the elastic parameters can be correlated to

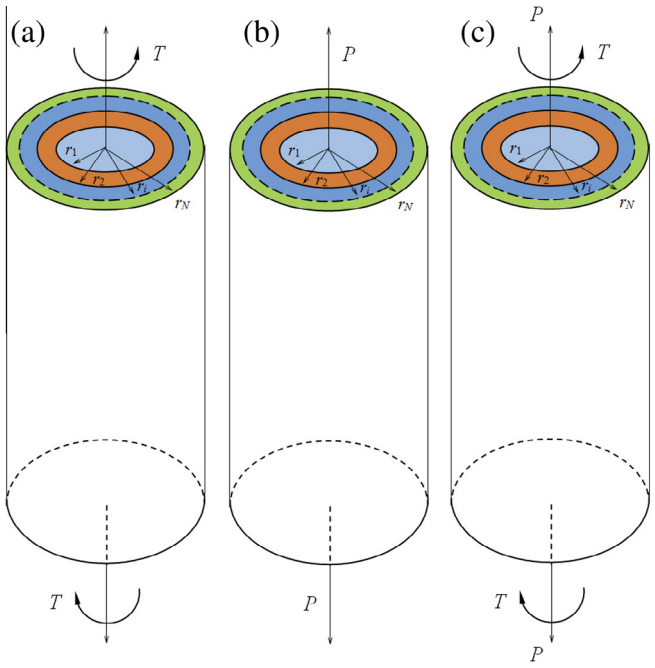

Fig. 1. A cylindrical composite consisting of N layers, with surfaces located at the radial coordinates, $r = r_i$, $i = 1, N$, under (a) torsion T, (b) axial loading P or (c) combined torsion T and axial loading P.

parameters of other models, e.g., via the comparison of the strain energy density to that of microstructural models based on mechanical and chemical contributions (Wu and Kirchner, 2010). Wang and Wu (2013a) have recently used the second-order model to study cylindrical multilayers under dilatational loadings.

The energy density W of Murnaghan (1951) is:

$$W = \frac{\lambda+2\mu}{2}J_1^2 - 2\mu J_2 + \frac{l+2m}{3}J_1^3 - 2mJ_1J_2 + nJ_3, \tag{2.1}$$

where λ and μ are the second-order and l, m, n the third-order elastic constants, respectively, and J_1, J_2, and J_3 are the strain invariants of the Lagrangian strain $\mathbf{E}$:

$$J_1 = E_1 + E_2 + E_3, \quad J_2 = E_1E_2 + E_2E_3 + E_3E_1, \quad J_3 = E_1E_2E_3. \tag{2.2}$$

The Lagrangian strain is expressed in terms of the deformation gradient as:

$$\mathbf{E} = \frac{1}{2}(\mathbf{F}^*\mathbf{F} - \mathbf{I}), \tag{2.3}$$

and the first Piola–Kirchhoff stress (relating forces in the current configuration to area vectors in the undeformed configuration, and generally non-symmetric) is defined as:

$$\mathbf{T} = \mathbf{F}\frac{\partial W}{\partial \mathbf{E}} = \mathbf{F}\left(\lambda J_1\mathbf{I} + 2\mu\mathbf{E} + \left(lJ_1^2 - 2mJ_2\right)\mathbf{I} + 2mJ_1\mathbf{E} + n\,co\mathbf{E}\right), \tag{2.4}$$

where $\mathbf{I}$ is the identity and co$\mathbf{E}$ represents the co-factor matrix of $\mathbf{E}$. The asterisk in $\mathbf{F}^*$ denotes the transpose.

We solve all the problems consistently, starting from the deformations and the equilibrium equations in terms of the first Piola–Kirchhoff stresses. The equilibrium equations in cylindrical coordinates in terms of the first Piola–Kirchhoff stresses are (Volokh, 2006):

$$\frac{\partial T_{rr}}{\partial r} - T_{\theta r}\frac{\partial \psi}{\partial r} + \frac{T_{rr}}{r} + \frac{\partial T_{r\theta}}{r\partial\theta} - \frac{T_{\theta\theta}}{r}\frac{\partial\psi}{\partial\theta} + \frac{\partial T_{rz}}{\partial z} - T_{\theta z}\frac{\partial\psi}{\partial z} = 0, \tag{2.5}$$

$$T_{rr}\frac{\partial\psi}{\partial r} + \frac{\partial T_{\theta r}}{\partial r} + \frac{T_{r\theta}}{r}\frac{\partial\psi}{\partial\theta} + \frac{T_{\theta R}}{r} + \frac{\partial T_{\theta\theta}}{r\partial\theta} + \frac{\partial T_{\theta z}}{\partial z} + T_{rz}\frac{\partial\psi}{\partial z} = 0, \tag{2.6}$$

$$\frac{\partial T_{zr}}{\partial r} + \frac{T_{zr}}{r} + \frac{\partial T_{z\theta}}{r\partial\theta} + \frac{\partial T_{zz}}{\partial z} = 0. \tag{2.7}$$

Strictly speaking, the component T_{rr} should be written as $T_{\rho r}$, which represents the stress along the ρ-direction in the deformed configuration with respect to the r-face in the undeformed configuration. Similarly, $T_{\theta r}$ should be written as $T_{\psi r}$ in the strict notation. As remarked by Volokh (2006), Lagrangian equilibrium equations in cylindrical and spherical coordinates are surprisingly "rarely discussed" in the literature, but they are of major interest in the mechanics of soft biomaterials. For simplicity, we will present the solutions for cylinders up to two layers only.

2.1. Pure torsion

Under torsion, the final coordinates (ρ, ψ, ζ) of the particle of a cylinder whose initial coordinates being (r, θ, z) are given by $(r + kF(r), \theta + k\alpha z + k^2G(z), z + kH(z))$, where $kF(r)$, $k\alpha z + k^2G(z)$, $kH(z)$ are the radial, angular and axial displacements respectively, with α denoting the angle of twist per unit length in the usual linear theory. Here k is a marker indicating the order of approximation of the theory; for second-order theory we retain terms up to k^2. The unknown radial displacement $kF(r) = k[F_1(r) + kF_2(r)]$, where $F_1(r)$ and $F_2(r)$ are respectively the first- and second-order terms. These terms are assumed to be functions of r only and not of z since all the sections are twisted in the same manner. The unknown second-order angular displacement $k^2G(z)$ is assumed to be a function of z, but will be shown to vanish, meaning that there is no additional twist under torsion in second-order elasticity theory. The unknown axial displacement $kH(z) = k[H_1(z) + kH_2(z)]$, where $H_1(z)$ and $H_2(z)$ are respectively the first- and second-order terms. These are taken to be functions of z only and not of r since the bar sections elongate or contract uniformly. This deformation representation for pure torsion permits displacements in both the axial and radial directions. The sign of the axial displacement determines the positive or negative Poynting effect.

Let $\mathbf{a}$ and $\mathbf{x}(\mathbf{a})$ denote the position vectors in the undeformed and deformed states, respectively. Their differentials are then:

$$d\mathbf{a} = \begin{pmatrix} dr \\ rd\theta \\ dz \end{pmatrix}, \quad d\mathbf{x} = \begin{pmatrix} (1+kF')dr \\ (r+kF)(d\theta + k\alpha dz + k^2G'dz) \\ (1+kH')dz \end{pmatrix}, \tag{2.8}$$

where the derivatives $F' = dF/dr = F_1'(r) + kF_2'(r)$, $G' = dG(z)/dz$ and $H' = dH/dz = H_1'(z) + kH_2'(z)$. The deformation gradient $\mathbf{F}$ is thus:

$$\mathbf{F} = \frac{d\mathbf{x}}{d\mathbf{a}} = \begin{pmatrix} 1+kF' & 0 & 0 \\ 0 & 1+\frac{kF}{r} & (r+kF)(k\alpha + k^2G') \\ 0 & 0 & 1+kH' \end{pmatrix}. \tag{2.9}$$

The stresses can be obtained by substituting Eq. (2.9) into Eq. (2.4). Substituting the stresses into Eqs. (2.5)–(2.7) with $\partial\psi/\partial r = 0$, $\partial T_{r\theta}/\partial\theta = 0$, $\partial\psi/\partial\theta = 1$ and $\partial\psi/\partial z = k\alpha + k^2G'$ yields two first-order and three second-order equilibrium equations as distinguished by the k and k^2 multipliers:

$$k\left(\frac{F_1''(r)}{r} + \frac{F_1'(r)}{r} - \frac{F_1'(r)}{r^2}\right) = 0, \tag{2.10}$$

$$kH_1''(z) = 0, \tag{2.11}$$

$$k^2\Big\{r^4\alpha^2(4m-3n+4\lambda-8\mu)-4(2l+2m+2\lambda+3\mu)F_1(r)^2 -4r(\lambda+2\mu)F_2(r)+4r^2(2l+2m+2\lambda+3\mu)F_1'(r)^2 +4r^2(\lambda+2\mu)F_2'(r)+4r^3(2l+\lambda)H_1'(z)F_1''(r)+4r(2l+\lambda)F_1(r)(-H_1'(z) +rF_1''(r))+4r^2F_1'(r)\big[(2l+\lambda)H_1'(z)+r(2l+4m+3\lambda+6\mu)F_1''(r)\big] +4r^3(\lambda+2\mu)F_2''(r)\Big\}=0, \tag{2.12}$$

$$k^2(r\alpha(m+\lambda+2\mu)H_1''(z)+\mu rG'(z)=0, \tag{2.13}$$

$$k^2\big\{(2l+\lambda)F_1(r)H_1''(z)+r\big[(2l+\lambda)F_1'(r)H_1''(z)+(2l+4m+3\lambda +6\mu)H_1'(z)H_1''(z)+(\lambda+2\mu)H_2''(z)\big]\big\}=0. \tag{2.14}$$

Note that the first-order term arising from Eq. (2.6) is identically satisfied, resulting in five equilibrium equations. We next solve these five equations for the unknown functions F_1, F_2, G, H_1 and H_2 for both the homogeneous and the two-layered cases. Solving the second-order equations requires the solutions of the first-order ones, as can be seen from the appearance of F_1 and H_1 in Eqs. (2.12)–(2.14).

2.1.1. Torsion of a bi-layered cylinder

2.1.1.1. First-order solutions. For an N-layered cylinder, the governing equilibrium equations are applied to each layer, and the form of the solutions is essentially identical to the homogeneous case. The essential difference lies in the requirement of interface continuity of the tractions and displacements for the N-layered problem. Considering a bi-layered cylinder, the solutions to Eqs. (2.10) and (2.11) for the first-order radial and axial displacements $F_1^{(i)}(r)$ and $H_1^{(i)}(r)$, $i=1,2$, are:

$$F_1^{(i)}(r)=F_{11}^{(i)}r+\frac{F_{12}^{(i)}}{r},\quad i=1,2, \tag{2.15}$$

$$H_1^{(i)}(z)=H_{11}^{(i)}z,\quad i=1,2, \tag{2.16}$$

where (i) indicates the layer and six unknown constants are to be determined. In addition, there are two twist rates α_1 and α_2 to be determined, resulting in a total of eight unknowns. For Layer 1, however, $F_{12}^{(1)}=0$ since the linear radial displacement vanishes at $r=0$. Note that $F_{12}^{(i)}\neq 0$ for $i=2$. Hence, there remain seven unknowns to be determined from the boundary conditions. For traction boundary conditions, the relevant tractions can be calculated from Eq. (2.4). The seven boundary conditions are:

(BC^{L}1) T_{rr}^L vanishes on the outer boundary $r=r_2$:

$$T_{rr}^{L(2)}(r=r_2)=0. \tag{2.17}$$

(BC^{L}2) No applied axial forces act at either end of the cylinder:

$$\int T_{zz}^{L(i)}(z=0,L)dA=0. \tag{2.18}$$

(BC^{L}3) The torsion applied to the cylinder is T:

$$\int T_{\theta z}^{L(i)}rdA=T. \tag{2.19}$$

(BC^{L}4) Linear radial displacement is continuous across the interface $r=r_1$:

$$F_1^{(1)}(r=r_1)=F_1^{(2)}(r=r_1). \tag{2.20}$$

(BC^{L}5) Linear circumferential displacement is continuous across the interface:

$$r_1\alpha_1 z=r_1\alpha_2 z,\quad \text{or}\quad \alpha_1=\alpha_2. \tag{2.21}$$

(BC^{L}6) Linear axial displacement is continuous across the interface:

$$H_{11}^{(1)}z=H_{11}^{(2)}z\quad\text{or}\quad H_{11}^{(1)}=H_{11}^{(2)}. \tag{2.22}$$

(BC^{L}7) Linear radial traction T_{rr}^L is continuous across the interface:

$$T_{rr}^{L(1)}(r=r_1)=T_{rr}^{L(2)}(r=r_1). \tag{2.23}$$

In the above equations, A is the area of either end of the cylinder. Also, $T_{\theta r}^{L(i)}=T_{zr}^{L(i)}=0$ identically according to Eq. (2.4) and only the continuity of T_{rr}^L needs to be enforced. Note that the second-order components $T_{\theta r}^{NL(i)}=T_{zr}^{NL(i)}=0$, and that these first and second-order shear stresses also vanish under pure axial and combined loadings.

With the constants determined, the linear displacement in the two layers can be written as:

$$u_r^{L(i)}=0,\quad u_\theta^{L(i)}=k\alpha rz=k\frac{2T}{\pi(r_1^4\mu_1-r_1^4\mu_2+r_2^4\mu_2)}rz,\quad u_z^{L(i)}=0, \tag{2.24}$$

where $\alpha_1=\alpha_2=\alpha=2T/\pi(r_1^4\mu_1-r_1^4\mu_2+r_2^4\mu_2)$. From Eq. (2.24), it can be seen that there are no radial and axial displacements in the first-order theory, with the latter implying that the Poynting effect does not exist in the first-order theory. Furthermore, the two layers rotate with the same angle so that a radius remains straight all the way from the cylinder center through the interface to the outer boundary.

The linear stresses can be written as:

$$\mathbf{T}^{L(i)}=\begin{pmatrix}0 & 0 & 0\\ 0 & 0 & k\frac{2rT\mu_i}{\pi\left(r_1^4(\mu_1-\mu_2)+r_2^4\mu_2\right)}\\ 0 & k\frac{2rT\mu_i}{\pi\left(r_1^4(\mu_1-\mu_2)+r_2^4\mu_2\right)} & 0\end{pmatrix}. \tag{2.25}$$

The non-vanishing shear stresses $T_{\theta z}^{L(i)}=T_{z\theta}^{L(i)}$ in the two layers are proportional to their respective shear modulus and they experience a jump at the interface. Also, T_{rr}^L turns out to be zero as well.

2.1.1.2. Second-order solutions. Moving on to the second-order theory, the solutions for the radial, angular and axial displacements $F_2^{(i)}(r)$, $G^{(i)}(z)$ and $H_2^{(i)}(z)$, $i=1,2$ can be derived as follows. Substituting $F_1^{(i)}(r)$, and $H_1^{(i)}(z)$ into the second-order equilibrium equations, i.e., Eqs. (2.12)–(2.14), $F_2^{(i)}(r)$, $G^{(i)}(z)$ and $H_2^{(i)}(z)$ can be determined as:

$$F_2^{(i)}(r)=-\frac{r^3T^2(4m_i-3n_i+4\lambda_i-8\mu_i)}{8\pi^2(r_1^4\mu_1-r_1^4\mu_2+r_2^4\mu_2)^2(\lambda_i+2\mu_i)}+F_{21}^{(i)}r+\frac{F_{22}^{(i)}}{r}, \tag{2.26}$$

$$G^{(i)}(z)=G_{11}^{(i)}z, \tag{2.27}$$

$$H_2^{(i)}(z)=H_{21}^{(i)}z, \tag{2.28}$$

for $i=1,2$. There are eight unknown constants $F_{21}^{(i)}$, $F_{22}^{(i)}$, $G_{11}^{(i)}$ and $H_{21}^{(i)}$. Again $F_{22}^{(1)}=0$ for the first layer. The following seven boundary conditions allow us to solve for the values of the seven remaining constants:

(BC^{NL}1) T_{rr}^{NL} vanishes at the outer surface:

$$T_{rr}^{NL(2)}(r=r_2)=0. \tag{2.29}$$

(BC^{NL}2) No applied forces act at either end of the cylinder:

$$\int T_{zz}^{NL(i)}(z=0,L)dA=0. \tag{2.30}$$

(BC^{NL}3) The contribution of the second-order shear stress $T_{\theta z}^{NL}$ to T is 0:

$$\int T_{\theta z}^{NL(i)}(z=0,L) r dA = 0. \tag{2.31}$$

(BC^{NL}4) Second-order radial displacement is continuous across the interface:

$$F_2^{(1)}(r=r_1) = F_2^{(2)}(r=r_1). \tag{2.32}$$

(BC^{NL}5) Second-order circumferential displacement is continuous across the interface:

$$G_{11}^{(1)} z = G_{11}^{(2)} z, \text{or } G_{11}^{(1)} = G_{11}^{(2)}. \tag{2.33}$$

(BC^{NL}6) Second-order axial displacement is continuous across the interface:

$$H_{21}^{(1)} z = H_{21}^{(2)} z, \text{or } H_{21}^{(1)} = H_{21}^{(2)}. \tag{2.34}$$

(BC^{NL}7) The nonlinear radial traction T_{rr}^{NL} is continuous across the interface:

$$T_{rr}^{NL(1)}(r=r_1) = T_{rr}^{NL(2)}(r=r_1). \tag{2.35}$$

It can be established that $G_{11}^{(1)} = G_{11}^{(2)} = 0$, thus $G^{(i)}(z) = 0$, which proves that there is no second-order twist under pure torsion. The five remaining constants $F_{21}^{(1)}$, $F_{21}^{(2)}$, $F_{22}^{(2)}$, $H_{21}^{(1)}$, $H_{21}^{(2)}$ are combinations of the material constants λ_i, μ_i, m_i, n_i, geometrical parameters r_i and the applied torsion T. Because of their complexities, they are not listed explicitly. They do not depend on l_i (only in the case of pure torsion). This reduced dependence on only four constants λ, μ, m and n is a consequence of the cylindrical symmetry of the problem.

2.1.1.3. Combined first- and second-order solutions. In summary, the components of the total displacement field (first- and second-order) can be written as:

$$\begin{aligned}
u_r^{(i)} &= k^2\left(-\frac{r^3T^2(4m_i-3n_i+4\lambda_i-8\mu_i)}{8\pi^2\left(r_1^4\mu_1-r_1^4\mu_2+r_2^4\mu_2\right)^2(\lambda_i+2\mu_i)} + F_{21}^{(i)} r + \frac{F_{22}^{(i)}}{r}\right),\\
u_\theta^{(1)} &= u_\theta^{(2)} = k\alpha r z = k\frac{2T}{\pi\left(r_1^4\mu_1-r_1^4\mu_2+r_2^4\mu_2\right)} r z,\\
u_z^{(1)} &= u_z^{(2)} = k^2 H_2^{(1)}(z) = k^2 H_2^{(2)}(z) = k^2 D z,
\end{aligned} \tag{2.36}$$

where D is defined as the Poynting effect coefficient for a bi-layered cylindrical composite:

$$\begin{aligned}
D = T^2\big(&-n_1r_1^4r_2^2\lambda_1\lambda_2 + n_2r_1^4r_2^2\lambda_1\lambda_2 - n_2r_2^6\lambda_1\lambda_2 - 4m_1r_1^4r_2^2\lambda_2\mu_1\\
&+3n_2r_1^4r_2^2\lambda_2\mu_1 - 2n_2r_1^2r_2^4\lambda_2\mu_1 - n_2r_2^6\lambda_2\mu_1 - 4r_1^4r_2^2\lambda_1\lambda_2\mu_1\\
&-8r_1^4r_2^2\lambda_2\mu_1^2 - n_1r_1^6\lambda_1\mu_2 + n_2r_1^6\lambda_1\mu_2 + 4m_2r_1^4r_2^2\lambda_1\mu_2 - n_1r_1^4r_2^2\lambda_1\mu_2\\
&-2n_2r_1^4r_2^2\lambda_1\mu_2 + n_2r_1^2r_2^4\lambda_1\mu_2 - 4m_2r_2^6\lambda_1\mu_2 + n_1r_1^6\lambda_2\mu_2 - n_2r_1^6\lambda_2\mu_2\\
&-n_1r_1^4r_2^2\lambda_2\mu_2 + n_2r_1^4r_2^2\lambda_2\mu_2 + n_2r_1^2r_2^4\lambda_2\mu_2 - n_2r_2^6\lambda_2\mu_2 + 4r_1^4r_2^2\lambda_1\lambda_2\mu_2\\
&-4r_2^6\lambda_1\lambda_2\mu_2 - 4m_1r_1^6\mu_1\mu_2 + 4m_2r_1^6\mu_1\mu_2 - 4m_1r_1^4r_2^2\mu_1\mu_2\\
&+4m_2r_1^4r_2^2\mu_1\mu_2 - 4m_2r_1^2r_2^4\mu_1\mu_2 - 4m_2r_2^6\mu_1\mu_2 - 4r_1^6\lambda_1\mu_1\mu_2\\
&-4r_1^4r_2^2\lambda_1\mu_1\mu_2 + 4r_1^6\lambda_2\mu_1\mu_2 + 20r_1^4r_2^2\lambda_2\mu_1\mu_2 - 20r_1^2r_2^4\lambda_2\mu_1\mu_2\\
&-4r_2^6\lambda_2\mu_1\mu_2 - 8r_1^6\mu_1^2\mu_2 - 8r_1^4r_2^2\mu_1^2\mu_2 + 4m_1r_1^6\mu_2^2 - 4m_2r_1^6\mu_2^2\\
&-4m_1r_1^4r_2^2\mu_2^2 + 4m_2r_1^4r_2^2\mu_2^2 + 4m_2r_1^2r_2^4\mu_2^2 - 4m_2r_2^6\mu_2^2 + 4r_1^6\lambda_1\mu_2^2\\
&-12r_1^4r_2^2\lambda_1\mu_2^2 + 16r_1^2r_2^4\lambda_1\mu_2^2 - 8r_2^6\lambda_1\mu_2^2 - 4r_1^6\lambda_2\mu_2^2 + 4r_1^4r_2^2\lambda_2\mu_2^2\\
&+4r_1^2r_2^4\lambda_2\mu_2^2 - 4r_2^6\lambda_2\mu_2^2 + 16r_1^6\mu_1\mu_2^2 - 8r_1^2r_2^4\mu_1\mu_2^2 - 8r_2^6\mu_1\mu_2^2\\
&-8r_1^6\mu_2^3 + 8r_1^4r_2^2\mu_2^3 + 8r_1^2r_2^4\mu_2^3 - 8r_2^6\mu_2^3\big)/\\
&\Big[4\pi^2\left(r_1^4\mu_1 - r_1^4\mu_2 + r_2^4\mu_2\right)^2\left(3r_1^2r_2^2\lambda_1\lambda_2\mu_1 + 2r_1^2r_2^2\lambda_2\mu_1^2\right.\\
&-3r_1^2r_2^2\lambda_1\lambda_2\mu_2 + 3r_2^4\lambda_1\lambda_2\mu_2 + 3r_1^4\lambda_1\mu_1\mu_2 + 3r_1^2r_2^2\lambda_1\mu_1\mu_2\\
&-3r_1^4\lambda_2\mu_1\mu_2 + 3r_2^4\lambda_2\mu_1\mu_2 + 2r_1^4\mu_1^2\mu_2 + 2r_1^2r_2^2\mu_1^2\mu_2 - 3r_1^4\lambda_1\mu_2^2\\
&+r_1^2r_2^2\lambda_1\mu_2^2 + 2r_2^4\lambda_1\mu_2^2 + 3r_1^4\lambda_2\mu_2^2 - 6r_1^2r_2^2\lambda_2\mu_2^2 + 3r_2^4\lambda_2\mu_2^2 - 4r_1^4\mu_1\mu_2^2\\
&\left.+2r_1^2r_2^2\mu_1\mu_2^2 + 2r_2^4\mu_1\mu_2^2 + 2r_1^4\mu_2^3 - 4r_1^2r_2^2\mu_2^3 + 2r_2^4\mu_2^3\right)\Big].
\end{aligned} \tag{2.37}$$

The radial and axial displacements represent second-order effects. Here, D is a very complex combination of the elastic constants, the radii and torsion applied of the two layers. This suggests that the overall Poynting effect of the composite may depend on the interface position in a nonlinear, and possibly unexpected manner, as shown later. Furthermore, the total stress field can be written as:

$$\mathbf{T}^{(i)} = \begin{pmatrix} k^2T_{rr}^{NL(i)} & 0 & 0\\ 0 & k^2T_{\theta\theta}^{NL(i)} & k\frac{2rT\mu_i}{\pi\left(r_1^4(\mu_1-\mu_2)+r_2^4\mu_2\right)}\\ 0 & k\frac{2rT\mu_i}{\pi\left(r_1^4(\mu_1-\mu_2)+r_2^4\mu_2\right)} & k^2T_{zz}^{NL(i)}\end{pmatrix}, \tag{2.38}$$

where the second-order normal stresses also assume complicated forms involving the material constants, the radii and the torsion. They are not written here explicitly due to their lengthiness but they can be computed easily.

2.1.2. Torsion of a homogeneous cylinder

The above results for a bi-layered cylinder can now be specialized for a homogeneous cylinder of radius R. By setting $\lambda_1 = \lambda_2 = \lambda$, $\mu_1 = \mu_2 = \mu$, $m_1 = m_2 = m$, $n_1 = n_2 = n$ in Eq. (2.36), the displacement field can be written as:

$$\begin{aligned}
u_r = &\frac{k^2}{8\pi^2R^8\mu^3(\lambda+2\mu)(3\lambda+2\mu)}\\
&\times\begin{pmatrix} rT^2\{n[3r^2\mu(3\lambda+2\mu)\\ +R^2(\lambda^2-5\lambda\mu-2\mu^2)]-4\mu[r^2(3\lambda^2-4\lambda\mu-4\mu^2)\\ +R^2(-\lambda^2+12\lambda\mu+12\mu^2)-R^2m(\lambda-2\mu)+r^2m(3\lambda+2\mu)]\}\end{pmatrix},
\end{aligned} \tag{2.39}$$

$$u_\theta = k\alpha r z, \tag{2.40}$$

$$u_z = -\frac{k^2T^2(n\lambda+4\mu(m+\lambda+2\mu))}{4\pi^2R^6\mu^3(3\lambda+2\mu)} z, \tag{2.41}$$

where $\alpha = 2T/\pi R^4\mu$ as in the usual linear theory for a homogeneous cylinder. Replacing T in Eq. (2.41) by α, the axial displacement can be written as $u_z = k^2Dz$, where

$$D = -\frac{T^2(n\lambda+4\mu(m+\lambda+2\mu))}{4\pi^2R^6\mu^3(3\lambda+2\mu)} \tag{2.42}$$

is the Poynting effect coefficient for the homogeneous cylinder. It can be seen that under pure torsion u_θ is first-order in nature while u_r and u_z represent second-order effects. In particular, u_z or D predicts the positive or negative Poynting effect while u_r predicts the associated radial expansion or contraction. The T^2 dependence in D implies that the direction of the torque does not influence the positive or negative nature of the Poynting effect. The sign of the effect is primarily determined by the relative values of the elastic constants. Note the strong inverse dependence on R^6. For a metal such as silver, the elastic constants are (Hirth and Lothe, 1982; Hiki and Granato, 1966): $\lambda = 91$ GPa, $\mu = 45$ GPa, $l = -265$ GPa, $m = -637$ GPa, and $n = 332$ GPa. Hence $D = 3.92\times10^{-4}T^2/\pi^2R^6$ by Eq. (2.42) and a positive Poynting effect

is predicted. The Poynting effect for other materials will be discussed in a subsequent section.

A similar specialization of Eq. (2.38) to the case of a homogeneous cylinder leads to the following five components for the stress field:

$$T_{rr}=\frac{k^2(r^2-R^2)T^2(n(2\lambda+\mu)+4\mu(m+5\lambda+6\mu))}{4\pi^2R^8\mu^2(\lambda+2\mu)}, \tag{2.43}$$

$$T_{\theta\theta}=\frac{k^2T^2(n(3r^2-R^2)(2\lambda+\mu)+4\mu(m(3r^2-R^2)-R^2(5\lambda+6\mu)+r^2(11\lambda+10\mu)))}{4\pi^2R^8\mu^2(\lambda+2\mu)}, \tag{2.44}$$

$$T_{zz}=\frac{k^2(2r^2-R^2)T^2(3n\lambda+8\mu(m+3\lambda+2\mu))}{4\pi^2R^8\mu^2(\lambda+2\mu)}, \tag{2.45}$$

$$T_{\theta z}=T_{z\theta}=\frac{2krT}{\pi R^4}. \tag{2.46}$$

The normal stresses, as represented by Eqs. (2.43)–(2.45), represent second-order effects, while the shear stress $T_{\theta z}=T_{z\theta}$ represents a first-order effect consistent with the usual linear theory. The normal stresses depend on both the second- and third-order elastic constants, while the shear stress does not depend on these constants at all.

2.2. Pure axial loading

Under the uniform axial stress P, the final coordinates (ρ,ψ,ζ) of the particle of the cylinder whose initial coordinates being (r,θ,z) are $(r+kF(r),\theta+kG(z),z+kH(z))$, where $kF(r),kG(z),kH(z)$ are respectively the radial, angular and axial displacements. The unknown radial displacement $kF(r)=k(F_1(r)+kF_2(r))$, where $F_1(r)$ and $F_2(r)$ are respectively the first- and second-order terms. These terms are assumed to be functions of r only and not of z since all the sections are axially loaded in the same manner. The unknown angular displacement $G(z)=G_1(z)+kG_2(z)$, where $G_1(z)$ and $G_2(z)$ are respectively the first- and second-order terms. They are taken to be functions of z, but will be shown to vanish identically in agreement with the physical reasoning that any twisting of the bar in one direction under an axial load will contradict with the axisymmetric nature of the axial load with respect to the circular cross-sections. A non-vanishing $kG(z)$ would have predicted an axial force–twist effect, i.e., twisting of the bar under axial loading. The unknown axial displacement $H(z)=H_1(z)+kH_2(z)$, where $H_1(z)$ and $H_2(z)$ are respectively the first- and second-order terms. These are taken to be functions of z only and not of r since the bar sections elongate or contract uniformly in the z-direction. This displacement field under tension permits displacements in all coordinate directions.

The differentials of position vectors $\mathbf{a}$ and $\mathbf{x}(\mathbf{a})$in undeformed and deformed states can be written respectively as:

$$d\mathbf{a}=\begin{pmatrix}dr\\ rd\theta\\ dz\end{pmatrix}\quad\text{and}\quad d\mathbf{x}=\begin{pmatrix}(1+kF')dr\\ (r+kF)(d\theta+kG'dz)\\ (1+kH')dz\end{pmatrix}, \tag{2.47}$$

where $F'=dF/dr=F_1'(r)+kF_2'(r)$, $G'=dG/dz=G_1'(z)+kG_2'(z)$, and $H'=dH/dz=H_1'(z)+kH_2'(z)$. The deformation gradient is thus:

$$\mathbf{F}=\frac{d\mathbf{x}}{d\mathbf{a}}=\begin{pmatrix}1+kF' & 0 & 0\\ 0 & 1+\frac{kF}{r} & (r+kF)kG'\\ 0 & 0 & 1+kH'\end{pmatrix}. \tag{2.48}$$

The stresses can be obtained by substituting Eq. (2.48) into Eq. (2.4). Substituting the stresses into Eqs. (2.5)–(2.7) with $\partial\psi/\partial r=0$, $\partial T_{r\theta}/\partial\theta=0$, $\partial\psi/\partial\theta=1$, $\partial\psi/\partial z=kG'$ yields three first-order and three second-order equilibrium equations as distinguished by the k and k^2 multipliers:

$$k\left(\frac{F_1''(r)}{r}+\frac{F_1'(r)}{r}-\frac{F_1'(r)}{r^2}\right)=0, \tag{2.49}$$

$$k\mu rG_1'(z)=0, \tag{2.50}$$

$$kH_1''(z)=0, \tag{2.51}$$

$$\begin{aligned}k^2\Big\{&-4(2l+2m+2\lambda+3\mu)F_1(r)^2+r^4(4m-3n+4\lambda-8\mu)G_1'(z)^2\\&+r\left[-4(\lambda+2\mu)F_2(r)-4(2l+\lambda)F_1(r)H_1'(z)\right]\\&+4r^2\Big[(2l+2m+2\lambda+3\mu)F_1'(r)^2+(\lambda+2\mu)F_2'(r)\\&+(2l+\lambda)F_1'(r)H_1'(z)+(2l+\lambda)F_1(r)F_1''(r)\Big]\\&+4r^3\left[(2l+4m+3\lambda+6\mu)F_1'(r)F_1''(r)+(2l+\lambda)H_1'(z)F_1''(r)\right.\\&\left.+(\lambda+2\mu)F_2''(r)\right]\Big\}=0,\end{aligned} \tag{2.52}$$

$$\begin{aligned}k^2\Big\{&(m+\lambda+3\mu)F_1(r)G_1''(z)+r\Big[\frac{1}{2}(2m-n+2\lambda)F_1'(r)G_1''(z)\\&+(m+\lambda+2\mu)H_1'(z)G_1''(z)+\mu G_2''(z)+(m+\lambda+2\mu)G_1'(z)H_1''(z)\Big]\Big\}=0,\end{aligned} \tag{2.53}$$

$$\begin{aligned}k^2\{&r^3(m+\lambda+2\mu)G_1'(z)G_1''(z)+(2l+\lambda)F_1(r)H_1''(z)\\&+r\left[(2l+\lambda)F_1'(r)H_1''(z)+(2l+4m+3\lambda+6\mu)H_1'(z)H_1''(z)\right.\\&\left.+(\lambda+2\mu)H_2''(z)\right]\}=0.\end{aligned} \tag{2.54}$$

These equilibrium equations can be solved for the unknown functions F_1, F_2, G_1, G_2, $H_1$and H_2, for both the homogeneous and the two-layered cases.

2.2.1. Axial loading of a bi-layered cylinder

2.2.1.1. First-order solutions. Considering a bi-layered cylinder as before, the first-order displacements and stresses can be obtained by solving Eqs. (2.49)–(2.51) with the boundary conditions (BC^L1)–(BC^L7). However, the summation of the axial forces acting at either end of the cylinder is $P\pi r_2^2$ in (BC^L2) and the torsion applied to the cylinder is zero in (BC^L3). The linear displacements in the two layers can be written as:

$$u_r^{L(1)}=kF_{11}^{(1)}r, \tag{2.55}$$

$$u_r^{L(2)}=k\left(F_{11}^{(2)}r+\frac{F_{12}^{(2)}}{r}\right), \tag{2.56}$$

$$u_\theta^{L(1)}=u_\theta^{L(2)}=rkG_{11}^1z=rkG_{11}^2z=0, \tag{2.57}$$

$$u_z^{L(1)}=u_z^{L(2)}=kH_{11}^{(1)}z=kH_{11}^{(2)}z, \tag{2.58}$$

where

$$F_{11}^{(1)}=-\frac{1}{2\xi_1}Pr_2^2\left[r_1^2(\lambda_1-\lambda_2)\mu_2+r_2^2(\lambda_2\mu_2+\lambda_1\lambda_2+\lambda_1\mu_2)\right], \tag{2.59}$$

$$F_{11}^{(2)}=-\frac{1}{2\xi_1}Pr_2^2\left[r_1^2(\lambda_1-\lambda_2)\mu_2+r_2^2\lambda_2(\lambda_1+\mu_1+\mu_2)\right], \tag{2.60}$$

$$F_{12}^{(2)}=\frac{1}{2\xi_1}Pr_1^2r_2^4(\lambda_2\mu_1-\lambda_1\mu_2), \tag{2.61}$$

$$G_{11}^{(1)}=G_{11}^{(2)}=0, \tag{2.62}$$

$$H_{11}^{(1)}=H_{11}^{(2)}=\frac{1}{\xi_1}Pr_2^2\left[r_1^2(\lambda_1-\lambda_2+\mu_1-\mu_2)\mu_2+r_2^2(\lambda_2+\mu_2)(\lambda_1+\mu_1+\mu_2)\right], \tag{2.63}$$

$$\begin{aligned}\xi_1 = (&r_1^4(3\lambda_1 - 3\lambda_2 + 2\mu_1 - 2\mu_2)(\mu_1 - \mu_2)\mu_2 \\ &+r_2^4\mu_2(\lambda_1 + \mu_1 + \mu_2)(3\lambda_2 + 2\mu_2) + r_1^2 r_2^2\big(\lambda_1\big(3\lambda_2(\mu_1 - \mu_2) \\ &+\mu_2(3\mu_1 + \mu_2)\big) + 2\big(\lambda_2(\mu_1^2 - 3\mu_2^2) + \mu_2\big(\mu_1^2 + \mu_1\mu_2 - 2\mu_2^2\big)\big)\big)\big).\end{aligned} \tag{2.64}$$

The linear stresses in Layer 1 can be written as:

$$\mathbf{T}^{L(1)} = \begin{pmatrix} k\left(H_{11}^{(1)}\lambda_1 + 2F_{11}^{(1)}(\lambda_1 + \mu_1)\right) & 0 & 0 \\ 0 & k(H_{11}^{(1)}\lambda_1 + 2F_{11}^{(1)}(\lambda_1 + \mu_1)) & 0 \\ 0 & 0 & k\left(2F_{11}^{(1)}\lambda_1 + H_{11}^{(1)}(\lambda_1 + 2\mu_1)\right) \end{pmatrix}. \tag{2.65}$$

$\mathbf{T}^{L(2)}$ in Layer 2 also has three diagonal terms only:

$$T_{rr}^{L(2)} = k\left(H_{11}^{(2)}\lambda_2 - \frac{2F_{12}^{(2)}}{r^2}\mu_2 + 2F_{11}^{(2)}(\lambda_2 + \mu_2)\right) \tag{2.66}$$

$$T_{\theta\theta}^{L(2)} = k\left(H_{11}^{(2)}\lambda_2 + \frac{2F_{12}^{(2)}}{r^2}\mu_2 + 2F_{11}^{(2)}(\lambda_2 + \mu_2)\right), \tag{2.67}$$

$$T_{zz}^{L(2)} = k\left(2F_{11}^{(2)}\lambda_2 + H_{11}^{(2)}(\lambda_2 + 2\mu_2)\right). \tag{2.68}$$

It can be seen that the bi-layered cylinder does not demonstrate an axial force–twist effect in the linear theory. Also, both Layers 1 and 2 undergo identical first-order axial displacements. Furthermore, the bi-layered composite has three non-vanishing first-order normal stress components. The existence of $T_{rr}^{L(i)}$ and $T_{\theta\theta}^{L(i)}$ shows the complex interaction of the two materials under pure axial loading, even in the linear theory. For instance, $T_{rr}^{L(2)} and T_{\theta\theta}^{L(2)}$ in Layer 2 vary with r while $T_{zz}^{L(1)}$ and $T_{zz}^{L(2)}$ are constant.

2.2.1.2. Second-order solutions. Consider next the second-order theory. Substituting $F_1^{(i)}(r), G_1^{(i)}(z)$ and $H_1^{(i)}(z)$ into the second-order governing equations Eqs. (2.52)–(2.54) and solving them with the boundary conditions (BC^{NL}1)–(BC^{NL}7), the second-order displacement and stress fields can be obtained. Specifically, the components of the total displacement field (first- and second-order) in the bi-layered cylinder can be written as:

$$u_r^{(i)} = k\left(F_{11}^{(i)}r + \frac{F_{12}^{(i)}}{r}\right) + k^2\left(\frac{(2m_i + \lambda_i + 3\mu_i)}{2r^3(\lambda_i + 2\mu_i)}\left(F_{12}^{(i)}\right)^2 + F_{21}^{(i)}r + \frac{F_{22}^{(i)}}{r}\right), \tag{2.69}$$

$$u_\theta^{(i)} = 0, \tag{2.70}$$

$$u_z^{(1)} = u_z^{(2)} = kH_{11}^{(1)}z + k^2H_{21}^{(1)}z = kH_{11}^{(2)}z + k^2H_{21}^{(2)}z. \tag{2.71}$$

The constants $F_{21}^{(1)}$, $F_{21}^{(2)}$, $F_{22}^{(2)}$, $H_{21}^{(1)} = H_{21}^{(2)}$ are complex combinations of material parameters λ_i, μ_i, l_i, m_i, n_i, geometrical parameters r_i and the applied axial loading P. Due to their lengthiness, they are not listed explicitly in this paper. It can be seen that the radial and axial displacements are not zero, while the circumferential displacement vanishes identically. There is no axial force–twist effect up to the second-order elasticity theory for a bi-layered composite under pure tension. This is also true for a multilayered composite. The combined stresses can be written as:

$$\mathbf{T}^{(i)} = \begin{pmatrix} kT_{rr}^{L(i)} + k^2T_{rr}^{NL(i)} & 0 & 0 \\ 0 & kT_{\theta\theta}^{L(i)} + k^2T_{\theta\theta}^{NL(i)} & 0 \\ 0 & 0 & kT_{zz}^{L(i)} + k^2T_{zz}^{NL(i)} \end{pmatrix}, \tag{2.72}$$

where the second-order normal stresses assume complicated forms involving the material parameters, the radii and the axial loading.

2.2.2. Axial loading of a homogeneous cylinder

Specializing Eqs. (2.69)–(2.71) for a homogeneous cylinder of radius R, the displacement field can be written as:

$$\begin{aligned}u_r &= kF(r) = kF_1(r) + k^2F_2(r) \\ &= -k\frac{P\lambda}{2\mu(3\lambda + 2\mu)}r + k^2\left(\frac{P\lambda}{2\mu(3\lambda + 2\mu)}\right)^2\gamma r,\end{aligned} \tag{2.73}$$

$$u_\theta = kG(z)r = kG_1(z)r + k^2G_2(z)r = 0, \tag{2.74}$$

$$u_z = kH(z) = kH_1(z) + k^2H_2(z) = k\frac{P}{E}z + k^2\delta\frac{P^2}{E^2}z, \tag{2.75}$$

where $E = \mu(3\lambda + 2\mu)/(\lambda + \mu)$ is the usual Young's modulus related to the Lamé constants λ and μ, and two new dimensionless constants are introduced as:

$$\gamma = \frac{n\lambda(3\lambda^2 + 6\lambda\mu + 4\mu^2) + \mu(9\lambda^3 + 18\lambda^2\mu - 8l\mu^2 + 8\lambda\mu^2)}{2\mu(3\lambda + 2\mu)\lambda^2}, \tag{2.76}$$

$$\delta = -\frac{3n\lambda^2(\lambda + \mu) + 2\mu[9\lambda^3 + 24\lambda^2\mu + 21\lambda\mu^2 + m(3\lambda + 2\mu)^2 + 2\mu^2(l + 3\mu)]}{4\mu(\lambda + \mu)^2(3\lambda + 2\mu)}. \tag{2.77}$$

Under pure axial loading, both the first- and second-order terms of u_θ vanish. Hence, no axial force–twist effect can occur. For u_r and u_z, the first-order components are linearly dependent on P, but the second-order ones are functions of P^2, implying that the second-order displacement changes in the radial and axial directions are independent of the direction of the axial loading. The dependence of these terms on P^2 implies that the second-order effect becomes increasingly important at larger axial loading. Lastly, the stress field for a homogeneous cylinder can be obtained by a specialization of Eq. (2.72), yielding:

$$\mathbf{T} = \begin{pmatrix} 0 & 0 & 0 \\ 0 & 0 & 0 \\ 0 & 0 & kP \end{pmatrix} \tag{2.78}$$

where the only non-vanishing component is T_{zz}, which does not have a second-order component.

2.3. Combined torsion-axial loading

Under combined torsion T and axial loading P, the final coordinates (ρ,ψ,ζ) of the particle of a cylinder whose initial coordinates being (r,θ,z) are assumed to be $(r+u_r,\theta+u_\theta/r,z+u_z)$, where the radial displacement $u_r=kF(r)$, the angular displacement $u_\theta/r=k\alpha z+kG(z)$ and the axial displacement $u_z=k(P/E)z+k^2(P/E)^2\delta z+kH(z)$. The radial displacement term $F(r)=F_1(r)+kF_2(r)$ captures any contribution due to T and P. In the angular term, $k\alpha z$ is the known linear contribution due to pure torsion (the second-order contribution is zero), and $G(z)=G_1(z)+kG_2(z)$ captures any other contribution such as pure axial loading and combined loading. Similarly, $k(P/E)z+k^2(P/E)^2\delta z$ in the axial term is the known linear and second-order contributions due to pure axial loading, and $H(z)=H_1(z)+kH_2(z)$ captures any other contribution. It is noted that $G(z)$ permits the additional rotation of a cylinder when an axial loading P is imposed, i.e., an axial force–twist effect may be possible. As shown previously, $G(z)=0$ for both homogeneous and bi-layered cylinders under pure loading modes. On the other hand, $H(z)$ permits an axial displacement under torsion and captures the Poynting effect.

Using a similar procedure as before, the deformation gradient $\mathbf{F}$ of the cylinder under combined torsion-axial loading can be obtained. The stresses are obtained by substituting $\mathbf{F}$ into Eq. (2.4). Using these stresses in Eqs. (2.5)–(2.7) with $\partial\psi/\partial r=0$, $\partial T_{r\theta}/\partial\theta=0$, $\partial\psi/\partial\theta=1$, $\partial\psi/\partial z=k\alpha+kG'$, we obtain three first-order and three second-order equilibrium equations which are omitted here for brevity.

2.3.1. Combined torsion-axial loading of a bi-layered cylinder

Consider the problem of the bi-layered cylinder. The displacements and stresses can be obtained by solving the equilibrium equations in conjunction with the boundary conditions (BC^L1)–(BC^L7) and ($BC^{NL}1$)–($BC^{NL}7$), appropriately modified.

The only necessary modification is made to (BC^L2), where the summation of the applied axial forces acting at either end of the cylinder is no longer zero but equal to $P\pi r_2^2$. The resulting total displacement field can be written as:

$$u_r^{(i)}=u_r^{(i)}(P)+u_r^{(i)}(T), \tag{2.79}$$

$$\begin{aligned}u_\theta^{(i)}&=u_\theta^{(i)}(P)+u_\theta^{(i)}(T)+k^2G_{21}^{(i)}rz\\&=k\frac{2T}{\pi(r_1^4\mu_1-r_1^4\mu_2+r_2^4\mu_2)}rz+k^2G_{21}^{(i)}rz,\end{aligned} \tag{2.80}$$

$$u_z^{(i)}=u_z^{(i)}(P)+u_z^{(i)}(T), \tag{2.81}$$

where $u_r^{(i)}(P)$, $u_\theta^{(i)}(P)=0$, $u_z^{(i)}(P)$ and $u_r^{(i)}(T)$, $u_\theta^{(i)}(T)$, $u_z^{(i)}(T)$ are the displacement components of the bi-layered cylinder under pure axial loading and pure torsion respectively. $G_{21}^{(i)}$, being a complex combination of λ_i, μ_i, m_i, n_i, r_i, P and T, is not listed explicitly. It can be seen that $u_r^{(i)}$ and $u_z^{(i)}$ are simple additions of the corresponding terms under pure torsion and pure axial loading, whereas $u_\theta^{(i)}$ is not. A non-vanishing coupled term $k^2G_{21}^{(i)}rz$ containing the product of T and P exists, meaning that the circumferential displacement will change by this value when an axial loading P is applied in the presence of a torsion T. This coupled term vanishes when $T=0$. Hence, although a coupled axial force–twist effect is not possible under pure axial loading, it is possible under combined torsion-axial loading.

The resulting total stress field can be written as:

$$\mathbf{T}^{(i)}=\mathbf{T}^{(i)}(P)+\mathbf{T}^{(i)}(T)+\begin{pmatrix}0&0&0\\0&0&k^2T_{\theta z}^{NL(i)}\\0&k^2T_{z\theta}^{NL(i)}&0\end{pmatrix}, \tag{2.82}$$

where $\mathbf{T}^{(i)}(P)$ and $\mathbf{T}^{(i)}(T)$ are the stress fields of the bi-layered cylinder under pure axial loading and pure torsion respectively. The shear stresses $T_{\theta z}^{NL(i)}$ and $T_{z\theta}^{NL(i)}$ are coupled in T and P and they are not equal. Their complex forms are not shown here.

2.3.2. Combined torsion-axial loading of a homogeneous cylinder

For the homogeneous cylinder, specialization of Eqs. (2.79)–(2.81) leads to the following total displacement field in explicit form:

$$\begin{aligned}u_r=kF(r)=kF_1(r)+k^2F_2(r)&=-\frac{kPr\lambda}{6\lambda\mu+4\mu^2}\\&+k^2\begin{pmatrix}\frac{1}{8\pi^2R^8\mu^3(\lambda+2\mu)(3\lambda+2\mu)}rT^2[4\mu(-(3r^2-R^2)\lambda(m+\lambda)\\-2(m(r^2+R^2)-2(r^2-3R^2)\lambda)\mu+4(r^2-3R^2)\mu^2)\\+n(3r^2\mu(3\lambda+2\mu)+R^2(\lambda^2-5\lambda\mu-2\mu^2))]\\+\frac{1}{8\mu^3(3\lambda+2\mu)^3}[P^2r(n\lambda(3\lambda^2+6\lambda\mu+4\mu^2)\\+\mu(9\lambda^3+18\lambda^2\mu-8l\mu^2+8\lambda\mu^2))]\end{pmatrix},\end{aligned} \tag{2.83}$$

$$\begin{aligned}u_\theta=kr\alpha z+krG(z)&=kr\alpha z+krG_1(z)+k^2rG_2(z)\\&=kr\frac{2T}{\pi R^4\mu}z-\frac{k^2PT(n\lambda+4\mu m+6\lambda\mu+8\mu^2)}{2\pi R^4\mu^3(3\lambda+2\mu)}rz,\end{aligned} \tag{2.84}$$

$$\begin{aligned}u_z=k\frac{P}{E}z+k^2\left(\frac{P}{E}\right)^2\delta z+kH(z)&=\frac{kP(\lambda+\mu)z}{\mu(3\lambda+2\mu)}\\&-\frac{1}{4\pi^2R^6\mu^3(3\lambda+2\mu)^3}\Big(k^2z\Big(n\lambda(3P^2\pi^2R^6\lambda(\lambda+\mu)\\&+T^2(3\lambda+2\mu)^2)+2\mu\Big(m(P^2\pi^2R^6+2T^2)(3\lambda+2\mu)^2\\&+2T^2(\lambda+2\mu)(3\lambda+2\mu)^2+P^2\pi^2R^6(9\lambda^3+24\lambda^2\mu\\&+(2l+21\lambda)\mu^2+6\mu^3)\Big)\Big)\Big).\end{aligned} \tag{2.85}$$

The radial, circumferential and axial displacements all contain linear and nonlinear parts. Importantly, u_θ has an additional coupled term $-(k^2PT(n\lambda+4\mu m+6\lambda\mu+8\mu^2)rz)/(2\pi R^4\mu^3(3\lambda+2\mu))$ in the expression, which shows the possibility of an axial force–twist effect, while $u_r^{(i)}$ and $u_z^{(i)}$ do not contain such coupled terms.

The total stress field can be obtained by specialization of Eq. (2.82), yielding the following explicit form:

$$T_{rr}=\frac{k^2(r-R)(r+R)T^2(n(2\lambda+\mu)+4\mu(m+5\lambda+6\mu))}{4\pi^2R^8\mu^2(\lambda+2\mu)}, \tag{2.86}$$

$$T_{\theta\theta}=\frac{k^2T^2(n(3r^2-R^2)(2\lambda+\mu)+4\mu(m(3r^2-R^2)-R^2(5\lambda+6\mu)+r^2(11\lambda+10\mu)))}{4\pi^2R^8\mu^2(\lambda+2\mu)}, \tag{2.87}$$

$$T_{zz}=kP+k^2\frac{(2r^2-R^2)T^2(3n\lambda+8\mu m+24\lambda\mu+16\mu^2)}{4\pi^2R^8\mu^2(\lambda+2\mu)}, \tag{2.88}$$

$$T_{\theta z}=k\frac{2Tr}{\pi R^4}, \tag{2.89}$$

$$T_{z\theta}=k\frac{2Tr}{\pi R^4}-k^2\frac{PTr}{\pi R^4\mu}, \tag{2.90}$$

with $T_{r\theta}=T_{\theta r}=0$ and $T_{rz}=T_{zr}=0$. Hence, the first Piola–Kirchhoff stress field in a homogeneous cylinder under combined torsion and axial loading is not symmetric because $T_{\theta z}$ is not equal to $T_{z\theta}$. There also exists a coupling term in $T_{z\theta}$. No coupling terms exist in all other stress components.

2.4. Summary of solutions

To illustrate clearly the first- and second-order terms in the displacement and stress components under pure torsion (T), pure axial loading (P) and combined loading (TP), the matrices for the three modes are respectively written in the following manner.

(a) Homogeneous cylinder:

$$\begin{pmatrix} u_r \\ u_\theta \\ u_z \end{pmatrix}_T = \begin{pmatrix} k^2 \\ k \\ k^2 \end{pmatrix}, \quad \begin{pmatrix} u_r \\ u_\theta \\ u_z \end{pmatrix}_P = \begin{pmatrix} k+k^2 \\ 0 \\ k+k^2 \end{pmatrix}, \quad \begin{pmatrix} u_r \\ u_\theta \\ u_z \end{pmatrix}_{TP} = \begin{pmatrix} k+k^2 \\ k+k^2 \\ k+k^2 \end{pmatrix}, \tag{2.91}$$

$$\mathbf{T}_T = \begin{pmatrix} k^2 & 0 & 0 \\ 0 & k^2 & k \\ 0 & k & k^2 \end{pmatrix}, \quad \mathbf{T}_P = \begin{pmatrix} 0 & 0 & 0 \\ 0 & 0 & 0 \\ 0 & 0 & k \end{pmatrix},$$
$$\mathbf{T}_{TP} = \begin{pmatrix} k^2 & 0 & 0 \\ 0 & k^2 & k+k^2 \\ 0 & k+k^2 & k+k^2 \end{pmatrix}. \tag{2.92}$$

(b) Bi-layered cylinder:

$$\begin{pmatrix} u_r \\ u_\theta \\ u_z \end{pmatrix}_T = \begin{pmatrix} k^2 \\ k \\ k^2 \end{pmatrix}, \quad \begin{pmatrix} u_r \\ u_\theta \\ u_z \end{pmatrix}_P = \begin{pmatrix} k+k^2 \\ 0 \\ k+k^2 \end{pmatrix},$$
$$\begin{pmatrix} u_r \\ u_\theta \\ u_z \end{pmatrix}_{TP} = \begin{pmatrix} k+k^2 \\ k+k^2 \\ k+k^2 \end{pmatrix}, \tag{2.93}$$

$$\mathbf{T}_T = \begin{pmatrix} k^2 & 0 & 0 \\ 0 & k^2 & k \\ 0 & k & k^2 \end{pmatrix}, \quad \mathbf{T}_P = \begin{pmatrix} k+k^2 & 0 & 0 \\ 0 & k+k^2 & 0 \\ 0 & 0 & k+k^2 \end{pmatrix},$$
$$\mathbf{T}_{TP} = \begin{pmatrix} k+k^2 & 0 & 0 \\ 0 & k+k^2 & k+k^2 \\ 0 & k+k^2 & k+k^2 \end{pmatrix}. \tag{2.94}$$

It can be seen that for combined loading, a direct superposition of the pure loading cases is generally not valid.

3. Numerical results

The section focuses on the influence of the interface position (denoted by $r = r_1$) and the elastic constants (λ_i, μ_i, l_i, m_i, n_i; $i = 1,2$) on the second-order stresses and displacements. We consider several soft materials whose elastic constants have been determined in comparison to the experimental data of soft materials, e.g., agar-gelatin (Catheline et al., 2003) and poly(acrylic acid) (PAA) gels (Wang and Wu, 2013b). For these two materials, the elastic constants λ, μ, l, m, n are 2.25×10^6, 8, -2×10^6, -20×10^6, 80 kPa, and 60, 12.21, −42.67, −35.60, −23.50 kPa, respectively. The large value of λ for the gelatin implies near incompressibility. In addition, we also consider several metallic materials whose elastic constants can be found in the works of Hirth and Lothe (1982), Hiki and Granato(1966), Hughes and Kelly (1953), Powell and Skove (1982) and Sindhu and Menon (2001).

For parametric studies, the elastic constants are varied from these reference values, and r_1 is also varied from 0 to the radius r_2 of the outer boundary. The applied torque assumes a magnitude of $T = 6 \times 10^{-10}$ or 10×10^{-10} kPa m^3, and the applied axial loading stress $P = 1.5$ or 0.1 kPa. The cylinder has the length $L = 0.01$ m, and an outer radius of $L/10$ or $L/5$. Table 1 lists all the elastic constants of the materials and the radii used in Figs. 2–10. The elastic parameters l_i are not needed for the case of torsion. The results for the pure and combined loadings are grouped in Sections 3.1 and 3.2, respectively.

3.1. Pure torsion or axial loading

3.1.1. Dependence of Poynting effect on elastic constants and interface position under torsion

Fig. 2 plots the $D = 0$ and $S = 0$ contours in the μ–n space for a soft cylinder of overall radius 0.002 m subjected to pure torsion. The variable S refers to the second-order radial displacement at the outer surface normalized with respect to the overall radius. In Fig. 2(a) and (b), the cylinders are homogeneous but with different elastic constants. In Fig. 2(c), the cylinder is a composite with Layers 1 and 2 respectively made of the materials in Fig. 2(a) and (b).

For the homogeneous cylinder in Fig. 2(a), the μ–n space (holding λ and m fixed) is seen to be partitioned into three regions, indicated by I, III and IV. Regions I and II indicate regions of positive Poynting effect ($D > 0$), but with $S > 0$ and $S < 0$, respectively. Regions III and IV indicate regions of negative Poynting effect ($D < 0$), but with $S > 0$ and $S < 0$, respectively. This figure shows the absence of Region II within the μ–n space, i.e., the homogeneous cylinder cannot elongate axially and contract radially within the parameter range investigated. Roughly speaking, the negative Poynting effect is predicted for negative and relatively small positive n in this case. In Fig. 2(b), however, Region I is missing and the homogeneous cylinder cannot elongate axially and expand radially at the same time.

The influence of inhomogeneity via the introduction of two concentric layers in the cylinder of the same overall size ($r_1 = 0.001$ m, $r_2 = 0.002$ m) is illustrated in Fig. 2(c). Here the $D = 0$ and $S = 0$ contours are plotted in the μ_2–n_2 space. All the elastic constants of Layer 1 (inner layer) are held fixed. Also, λ_2 and m_2 of Layer 2 are held fixed at the same values as those of the homogeneous material in Fig. 2(b). For the same range of parameter values, it can be seen that the regions in Fig. 2(a) and (b) have fused and rearranged themselves so that all four regions are now present. Given the existence of the four regions, there will be either volumetric expansion or contraction of the cylinder in general. This figure shows the possibility of using elastic inhomogeneity to design for an overall positive or negative Poynting effect with radial (or volumetric) expansion or contraction in a cylinder under torsion.

Fig. 3(a)–(c) plot the variation of D with r_1 for three materially different soft composites of the same overall size ($r_2 = 0.002$ m, $L = 0.01$ m) subjected to the torque $T = 6 \times 10^{-10}$ kPa m^3. In each sub-figure, the solid and dotted lines denote respectively the results for a composite and its reverse configuration, i.e., the materials of Layers 1 and 2 are interchanged in the two composites. At $r_1 = 0$, the composite degenerates into a homogeneous cylinder made up completely of Layer 2 material. Similarly, at $r_1 = r_2$ the homogeneous cylinder is composed of the material of Layer 1.

Several interesting and unusual phenomena can be observed. First, the curve may not vary monotonically between the two end points $r_1 = 0$ and $r_1 = r_2$, implying that the Poynting effect is *amplified* beyond that of the homogenous cylinders. This is evident in Fig. 3(a) and (b), but not in Fig. 3(c). As a case in point, consider the solid line of Fig. 3(b), where $D \simeq +0.13 \times 10^{-5}$ and -0.83×10^{-5} for homogeneous cylinders of Layers 2 and 1, respectively. Joining these two materials into a composite of the same overall size, however, may result in $D \simeq -2 \times 10^{-5}$, depending on the interface position. Second, the order in which the two materials are placed in the composite may also strongly influence the Poynting effect. In Fig. 3(b), reversing the layer materials un the composite results in $D \simeq -3.8 \times 10^{-5}$ (dotted line), almost twice

Table 1
Elastic, geometrical and loading parameters used in Figs. 2–10.

	Material 1 Material 2	λ_1 λ_2	μ_1 μ_2	m_1 m_2	n_1 n_2	r_1	r_2	L	T	P
Fig. 2(a)	Agar-gelatin-based	2.25×10^6		-20×10^6		2		10	0.6	
Fig. 2(b)	PAA gel-based	60		−42.67		2		10	0.6	
Fig. 2(c)	Agar-gelatin-based	2.25×10^6	8	-20×10^6	80	1	2	10	0.6	
	PAA gel-based	60		−42.67						
Fig. 3(a) solid	Agar-gelatin-based	2.5×10^4	2000	-20×10^6	8		1	10	0.6	
	Polymer-based	1000	200	−2450	−2350					
Fig. 3(a) dashed	Polymer-based	1000	200	−2450	−2350		1	10	0.6	
	Agar-gelatin-based	2.5×10^4	2000	-20×10^6	8					
Fig. 3(b) solid	Agar-gelatin-based	2.25×10^6	800	10^9	8		1	10	0.6	
	Polymer-based	1000	200	−2450	−2350					
Fig. 3(b) dashed	Polymer-based	1000	200	−2450	−2350		1	10	0.6	
	Agar-gelatin-based	2.25×10^6	800	10^9	8					
Fig. 3(c) solid	Agar-gelatin	2.25×10^6	8	-20×10^6	80		1	10	0.6	
	NIPA/SA gel-based	40	3.983	−32.44	−2000					
Fig. 3(c) dashed	NIPA/SA gel-based	40	3.983	−32.44	−2000		1	10	0.6	
	Agar-gelatin-based	2.25×10^6	8	-20×10^6	80					
Fig. 4(a) solid	Ag	91×10^3	45×10^3	-637×10^3	332×10^3		1	10	0.6	
	Cu	121×10^3	75.5×10^3	-780×10^3	-380×10^3					
Fig. 4(a) dashed	Cu	121×10^3	75.5×10^3	-780×10^3	-380×10^3		1	10	0.6	
	Ag	91×10^3	45×10^3	-637×10^3	332×10^3					
Fig. 4(b) solid	Al	60.41×10^3	28.34×10^3	-383.9×10^3	15.4×10^3		1	10	0.6	
	Cu	121×10^3	75.5×10^3	-780×10^3	-380×10^3					
Fig. 4(b) dashed	Cu	121×10^3	75.5×10^3	-780×10^3	-380×10^3		1	10	0.6	
	Al	60.41×10^3	28.34×10^3	-383.9×10^3	15.4×10^3					
Fig. 4(c) solid	TiAl	105×10^3	120×10^3	-40×10^3	-160×10^3		1	10	0.6	
	Fe	110×10^3	82×10^3	-1030×10^3	1100×10^3					
Fig. 4(c) dashed	Fe	110×10^3	82×10^3	-1030×10^3	1100×10^3		1	10	0.6	
	TiAl	105×10^3	120×10^3	-40×10^3	-160×10^3					
	Material 1 Material 2	λ_1 λ_2	μ_1 μ_2	l_1 l_2	m_1 m_2	n_1 n_2	r_1	r_2	L	T	P
Fig. 5(a), (b)	Cardiomyocyte-based	111.812		7.016×10^2	2.65×10^3	−20	1	2	10		1.5
	Agar-gelatin-based	2.25×10^6		-2×10^6	-20×10^6	80					
Fig. 6(a), (b) solid	Agar-gelatin	2.25×10^6	8	-2×10^6	-20×10^6	80		1	10		0.1
	Cardiomyocyte	111.812	2.282	7.016×10^2	2.65×10^3	−20					
Fig. 6(a), (b) dashed	Cardiomyocyte	111.812	2.282	7.016×10^2	2.65×10^3	−20		1	10		0.1
	Agar-gelatin	2.25×10^6	8	-2×10^6	-20×10^6	80					
Fig. 7(a)	Agar-gelatin	2.25×10^6	8	-2×10^6	-20×10^6	80	1	2	10	1	1
	PAA gels-based	60		−42.67	−35.60						
Fig. 7(b)	Ag	91×10^3	45×10^3	-265×10^3	-637×10^3	332×10^3	1	2	10	1	1
	Cu-based	121×10^3		-407×10^3	-780×10^3						
Fig. 8(a), (b)	Agar-gelatin	2.25×10^6	8	-2×10^6	-20×10^6	80		1	10	1	0.1
	PAA gels	60	12.21	−42.67	−35.60	−23.50					
Fig. 9(a)	Agar-gelatin	2.25×10^6	8	-2×10^6	-20×10^6	80		1	10	1	0.1
	PAA gels	60	12.21	−42.67	−35.60	−23.50					
Fig. 9(b)	Cu	121×10^3	75.5×10^3	-407×10^3	-780×10^3	-380×10^3		1	10	1	0.1
	Ag	91×10^3	45×10^3	-265×10^3	-637×10^3	332×10^3					
Fig. 10	Myocardial core	32670	3.3	-2.25×10^6	−360	20	0.525	0.55			
	Endocardial sheath	4076	7.0	-2×10^4	−4200	−46					

Note: poly(acrylic acid) = PAA, *N*-isopropylacrylamide = NIPA, sodium acrylate = SA.
Units: λ, μ, l, m, n (kPa); r_1, r_2, L (μm); T (10^{-9} kPa·m^3 = 1 mN·mm); P (kPa = 1mN/mm^2).

that of the original configuration. Third, this amplification effect is not always present. Fig. 3(c) is an example of two materials whose composite does not have a Poynting effect stronger than the homogeneous ones. Finally, a minor point is that there may exist multiple interface positions where the Poynting effect is the same regardless of the order of the layers, as indicated by the intersection of the solid and dotted curves.

We further explore the above behaviors for several metallic composites. Fig. 4 plots the results for three different metal combinations. The metals in Layers 1 and 2 are silver and copper, aluminum and copper, and TiAl alloy and Armco iron for the solid lines in the three sub-figures, respectively. The dotted lines show the results for the reverse configurations. It can be observed that the curves vary monotonically between their end points; there is no amplification of the Poynting effect. Another point worthy of note is that D is of the order of 10^{-11} to 10^{-12}, much smaller compared to the range of 10^{-2} to 10^{-5} for the soft materials investigated in Fig. 3. For a homogeneous cylinder of TiAl intermetallic, D is negative as shown in Fig. 4(c).

3.1.2. Dependence of second-order effects on elastic constants and interface position under axial loading

With reference to Fig. 5, a two-layer soft composite ($r_1 = 0.001$ m, $r_2 = 0.002$ m, $L = 0.01$ m) is subjected to pure axial loading $P = 1.5$ kPa. The material constants of the two layers are held fixed and listed in Table 1, except for μ_1 and μ_2 which are varied to show their influence on the stresses T_{zz} on either side of the interface $r = r_1$. In Fig. 5(a) and (b), the contours T_{zz} ($r = r_1^+$) = 0 and T_{zz} ($r = r_1^-$) = 0 are shown respectively in the μ_1–μ_2 space. The symbols r_1^+ and r_1^- denote radial positions in Layers 2 and 1, respectively. These interfacial stresses are not functions of θ and z, and can be computed from Eq. (2.72). There exist Regions I and II

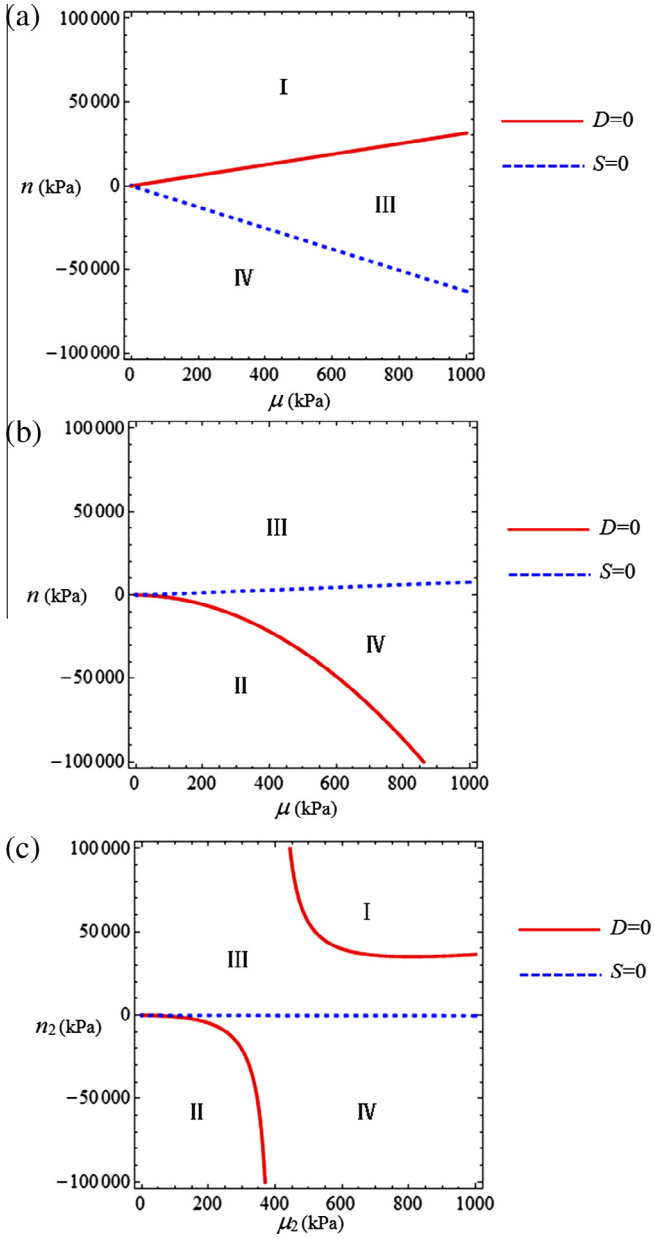

Fig. 2. Contours of the Poynting effect coefficient $D = 0$ (solid line) and radial displacement $S = 0$ (dashed line) in (a) μ–n space for a homogeneous cylinder, (b) μ–n space for a different homogeneous cylinder, and (c) μ_2–n_2 space for a two-layer composite cylinder under torsion.

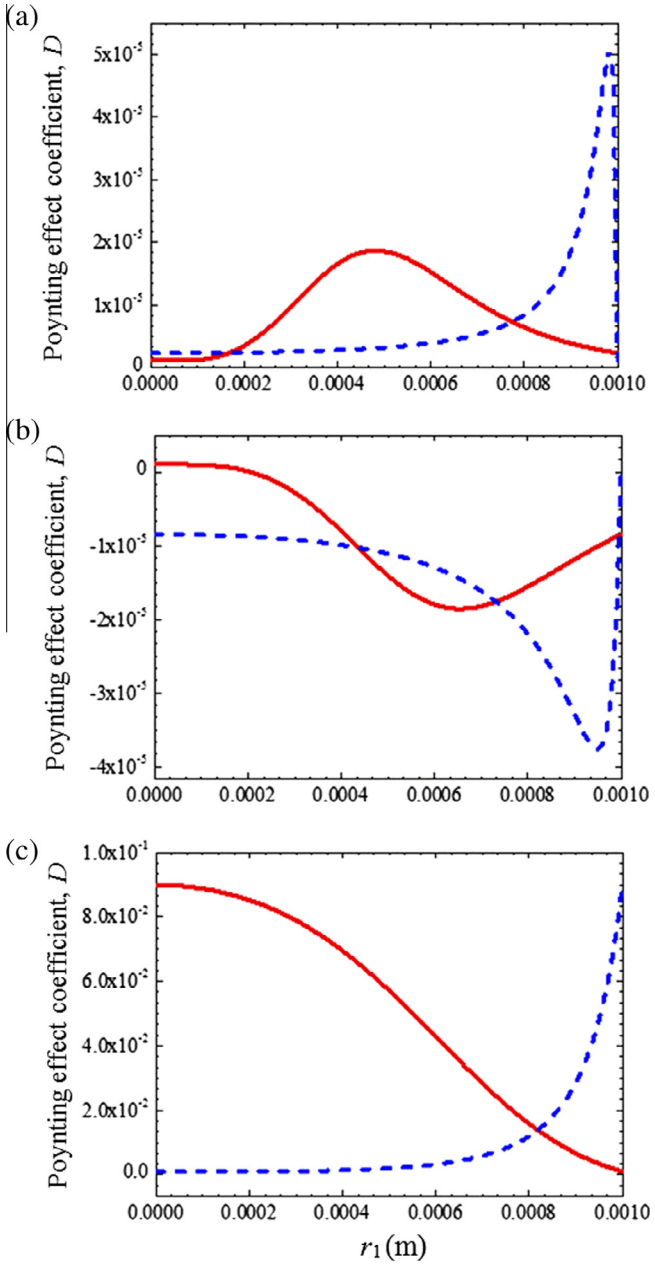

Fig. 3. Variation of the Poynting effect coefficient D with the interface position r_1 for three different two-layer composites (solid line) and their reverse configurations (dashed line) under pure torsion. The materials for (a)–(c) are listed in Table 1.

within which T_{zz} is either positive or negative, respectively, unlike the purely homogeneous case where only the first-order component $T_{zz} = kP$ exists and is constant throughout the cylinder. There are both k and k^2 normal stresses in a composite cylinder under axial loading. Also, $T_{zz}(r = r_1^+)$ and $T_{zz}(r = r_1^-)$ are not equal, as implied by the differences in the curves shown in the two sub-figures. The dependence on the elastic constants is complex; for instance there are two values of μ_1 for a given μ_2 for which $T_{zz}(r = r_1^+) = 0$, as indicated by the loop in Fig. 5(a).

We investigate how the second-order radial displacement u_r^{NL} at the outer boundary and the second-order axial displacement u_z^{NL} at the top end, vary with the interface position of a two-layer composite and its reverse configuration. The cylinders ($r_2 = 0.001$ m, $L = 0.01$ m) are subjected to the axial loading of $P = 0.1$ kPa, and their elastic constants are given in Table 1. Fig. 6(a) plots $u_r^{NL}(r_2)/r_2$ versus r_1, while Fig. 6(b) $u_z^{NL}(L)/L$ versus r_1. Both displacements vary nonlinearly with r_1, but $u_r^{NL}(r_2)/r_2$ in a non-monotonic and $u_z^{NL}(L)/L$ in a monotonic manner. In particular, the second-order radial displacement of the composite may be significantly larger than that of its homogeneous counterparts. This is similar to the Poynting effect of a composite and its homogeneous counterparts under pure torsion. Fig. 6(b) shows that the axial displacement does not display this amplification effect, however.

3.2. Combined torsion and axial loading

3.2.1. Dependence of axial force–twist effect on elastic constants and interface position

Fig. 7 plots the constant second-order circumferential displacement $u_\theta^{NL}(z = L) = 0$ curves in the μ_2–n_2 space for (a) a bi-layered composite of soft materials and (b) a metallic composite. The other

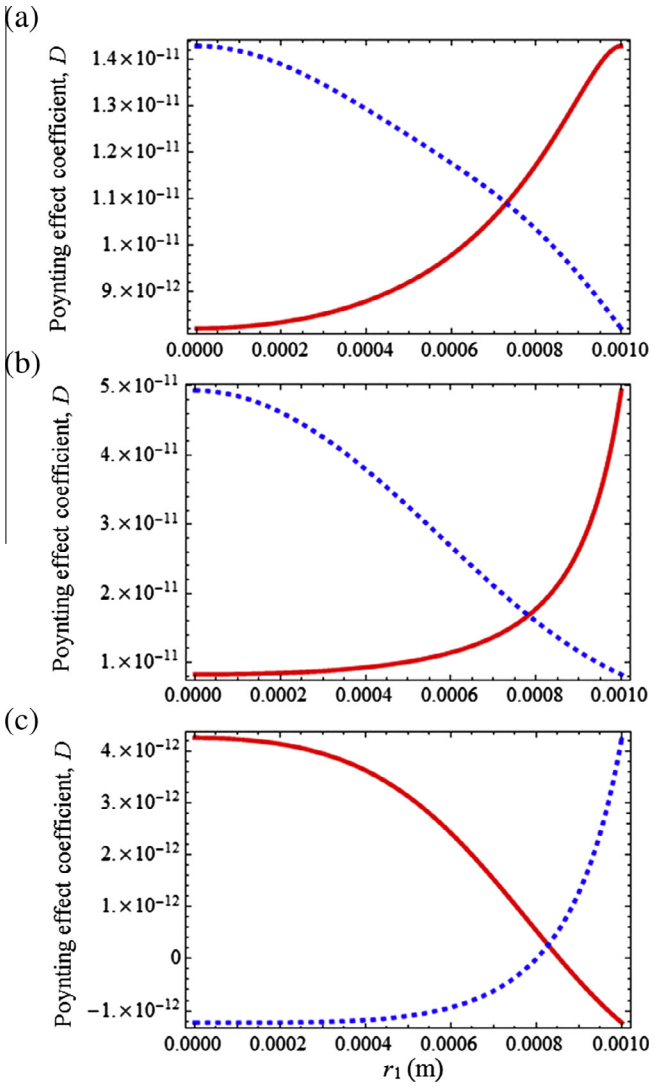

Fig. 4. Variation of the Poynting effect coefficient D with the interface position r_1 for three different two-layer composites of metals (solid line) and reverse configurations (dashed line) under pure torsion: (a) silver/copper, (b) aluminum/copper, and (c) TiAl/Armco iron.

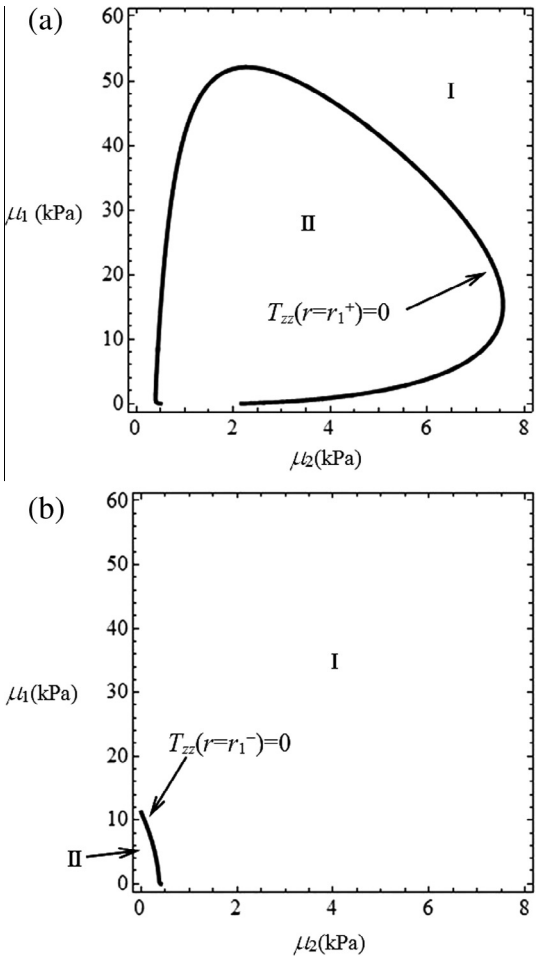

Fig. 5. Contours of the constant interfacial axial stress (a) $T_{zz}(r = r_1^+) = 0$ and (b) $T_{zz}(r = r_1^-) = 0$ in μ_2–μ_1 space for a two-layer composite under axial loading $P = 1.5$ kPa.

elastic parameters are held fixed and listed in Table 1. This displacement component is a coupled term (depending on both T and P) while the linear component is solely dependent on T, as shown in Eq. (2.80). The cylinder parameters are $r_1 = 0.001$ m, $r_2 = 0.002$ m and $L = 0.01$ m. The torque $T = 10 \times 10^{-10}$ kPa m^3 and $P = 1$ kPa.

In Fig. 7(a), the μ_2–n_2 space is seen to be partitioned into two regions, indicated by I and II, which means positive and negative $u_\theta^{NL}(z = L)$, respectively. By varying μ_2 and n_2, $u_\theta^{NL}(z = L)$ can be positive or negative, implying that the twisting angle may increase (positive axial force–twist effect) or decrease (negative axial force–twist effect) when an axial loading P is imposed on the cylinder under a torsion T. Roughly speaking, the positive effect is achieved when $\mu_2 < 350$ kPa and $n_2 < 0$ kPa or $\mu_2 > 450$ kPa and $n_2 > 50000$ kPa. Fig. 7(a) illustrates the possibility of designing a biomaterial composite with positive or negative axial force–twist effect via elasticity.

In order to compare the different dependences of the axial force–twist effect for composites of soft biomaterials and metallic materials, Fig. 7 (b) is presented. Here the $u_\theta^{NL}(z = L) = 0$ contour is also plotted in the μ_2–n_2 space. The material in Layer 1 is chosen to be silver, and λ_2 and m_2 of Layer 2 is chosen from the values for copper with μ_2 and n_2 varied in the simulation. It can be seen that Regions I and II are very different from those shown for the soft composite. Generally speaking, the positive axial force–twist effect is obtained for negative values of n_2, depending on m_2, with $\mu_2 < 6 \times 10^5$ kPa as indicated by Region I. Thus for soft and metallic composites, Fig. 7 shows the great difference between their dependences of the axial force–twist effect on the elastic parameters.

It should be mentioned that the axial force–twist effect in soft composites under combined loading cannot be ignored. Results not included here show that the coupled angular displacement is generally one order of magnitude less than the angular displacement due to pure torsion. Moreover, the coupled term is proportional to P and it will become larger for a larger P. In contrast, the axial force–twist effect in metals is not obvious, with the coupled angular displacement about five orders of magnitude less than the angular displacement due to pure torsion.

3.2.2. Dependence of second-order displacements on interface position

An interesting question is the relative importance of torsion versus axial loading when a soft composite is subjected to combined loading. This is investigated in Fig. 8(a), which plots the variation of $u_r^{NL}(P)/u_r^{NL}(T)$ versus r_1, where $u_r^{NL}(P)$ and $u_r^{NL}(T)$ denote the contributions due to P and T, respectively, to the second-order radial displacement, i.e., $u_r^{NL} = u_r^{NL}(P) + u_r^{NL}(T)$. Similarly, Fig. 8(b) plots $u_z^{NL}(P)/u_z^{NL}(T)$ versus r_1, where the second-order axial displacement is made up of the contributions from P and T, i.e.,

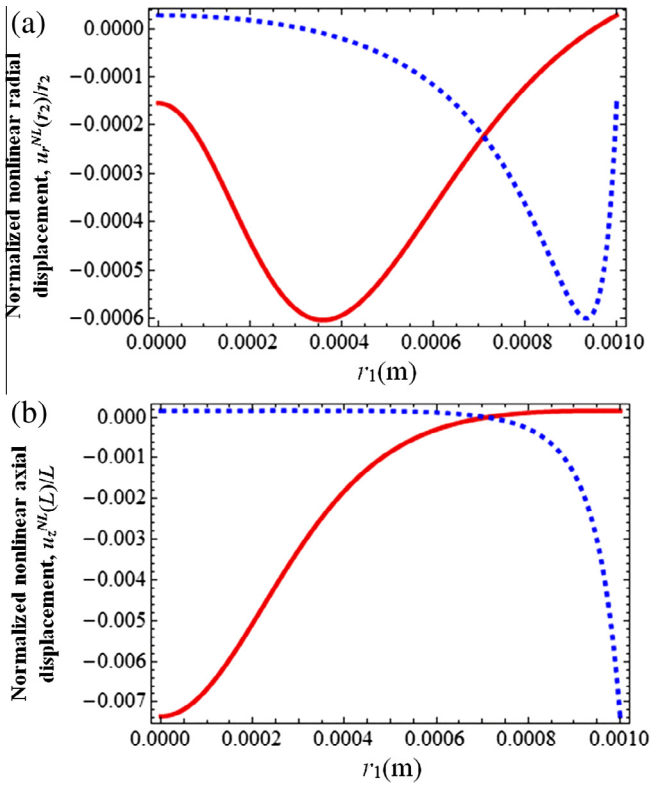

Fig. 6. Variation of normalized second-order (a) radial displacement $u_r^{NL}(r_2)/r_2$, and (b) axial displacement $u_z^{NL}(L)/L$ with the interface position r_1 for two different two-layer composites under axial loading $P = 0.1$ kPa.

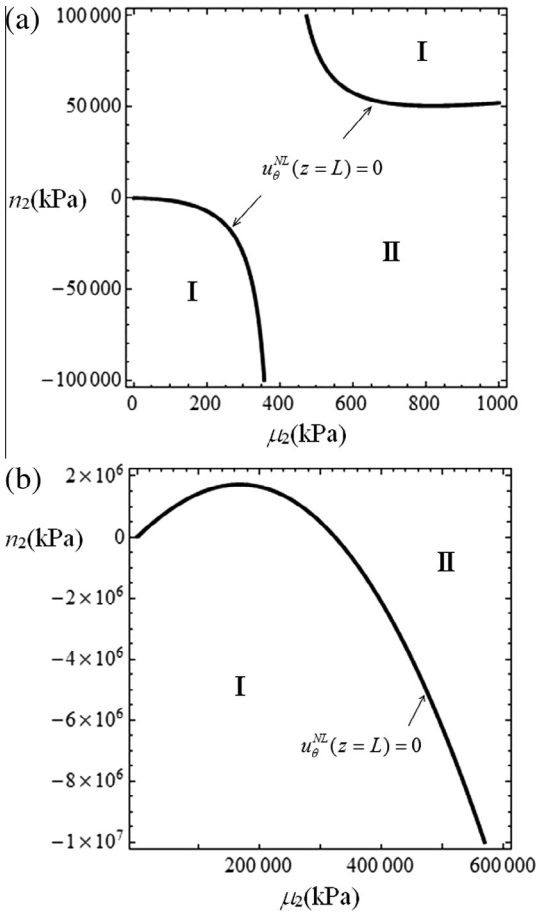

Fig. 7. Contours of the second-order coupled circumferential displacement $u_\theta^{NL}(z=L)=0$ in μ_2–n_2 space for: (a) soft composite and (b) metallic composite. Positive and negative axial force–twist effects are predicted for Regions I and II, respectively.

$u_z^{NL} = u_z^{NL}(P) + u_z^{NL}(T)$. In this figure, the composite is subjected to $T = 10 \times 10^{-10}$ kPa m^3 = 1 mN mm and $P = 1$ kPa = 1 mN/mm^2.

It can be observed that when r_1 increases, the ratio $u_r^{NL}(P)/u_r^{NL}(T)$ increases from negative to positive monotonically in Fig. 8 (a). Also, T dominates over P if a composite is made up of roughly equal amount of the different materials, but P dominates over T if the composite is made up of a large core with a thin outer layer or a small core with a thick outer layer. The relative contributions of P and T can also differ in sign. In Fig. 8(b), there exists a singular point when $r_1 \approx 0.0002$ m, around which the contribution of T to axial displacement nearly vanishes and the contribution of P dominates. This merely means that the Poynting effect disappears for this composite with interface located at $r_1 \approx 0.0002$ m. The results shown here naturally also depend on the relative magnitudes of T and P.

3.2.3. Dependence of second-order stresses on interface position

A bi-layered composite is subjected to the combined loading $T = 10 \times 10^{-10}$ kPa m^3 and $P = 1$ kPa. The variations of the second-order *coupled* terms in the shear stress components $T_{\theta z}(r = r_1^-)$ and $T_{z\theta}(r = r_1^-)$ with r_1 are plotted for soft and metal composites in Fig. 9(a) and (b), respectively. The metallic composite is made up of copper in Layer 1 and silver in Layer 2.

A number of observations can be made. The coupled terms in $T_{\theta z}(r = r_1^-)$ and $T_{z\theta}(r = r_1^-)$ are not equal. Both do not vary monotonically between the end points $r_1 = 0$ and $r_1 = r_2$ and will achieve an extremum at certain values of r_1. The end points represent homogeneous materials. Thus, although two homogeneous materials have zero or small second-order effects, their composites may have such effects significantly amplified. Moreover, these effects in the soft composite are much larger than those in the metallic composite, with magnitudes of the order of 10^{-2} and 10^{-6} kPa, respectively, as compared to the loading of $P = 1$ kPa.

3.2.4. Comparison with experimental data

In Fig. 10, the prediction of the twisting moment T and the average axial stress P of the second-order model versus the twist per unit length (twist rate) is compared to the experimental data of Criscione et al. (1999) for finite extension and torsion on cardiac papillary muscles. This muscle is considered as a composite of a myocardium core and a thin endocardium sheath, with an overall radius in the range of 0.375 to 0.65 mm and a sheath thickness of less than 25 μm. Since it is transversely isotropic, the second-order isotropic model here should be regarded as an approximation. The finite extension is held fixed at a stretch ratio of 1.04. Fig. 10(a) and (b) plot T and P versus the twist per unit length. The elastic constants for the two materials used in the simulation are listed in Table 1. The shear moduli μ_i are of the order of 10 kPa, with λ_i calculated assuming near-incompressibility. The third-order elastic constants are adjusted to fit the test data. The torque-twist rate prediction appears to overestimate the data (a larger T is predicted for a given twist rate), while the axial stress-twist rate prediction fits the data reasonably well. The analytical expressions for T and P are solved from the equilibrium equations; they are not arbitrary expressions with a number of fitting constants which can be calibrated against the data. The discrepancy between theory and data may be attributed to the assumption of complete isotropy in the theory, while the test specimens are actually transversely isotropic with the property in the longitudinal direction different from that

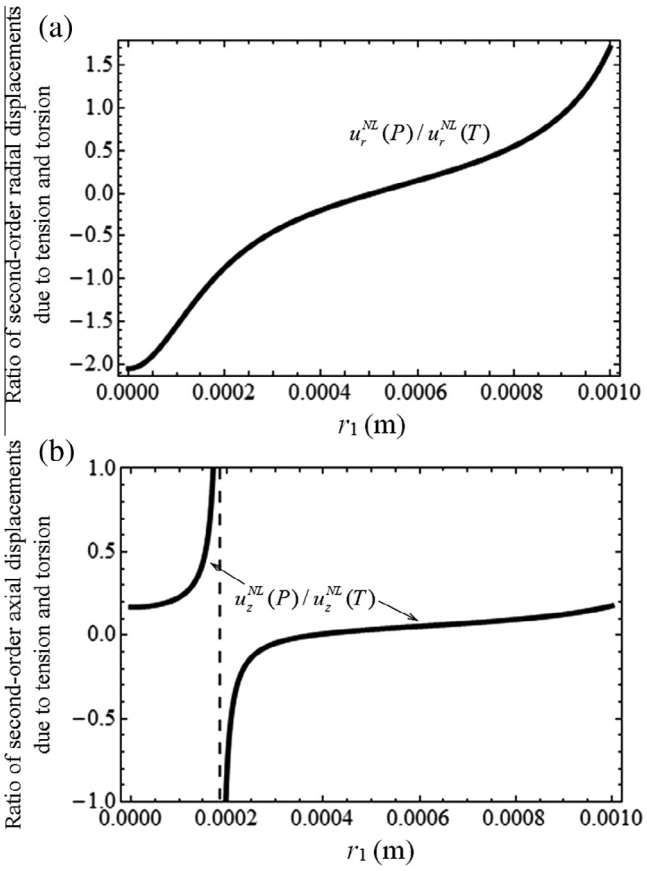

Fig. 8. Variation of (a) the ratio $u_r^{NL}(P)/u_r^{NL}(T)$ of the second-order radial displacements at the outer boundary, and (b) the ratio $u_z^{NL}(P)/u_z^{NL}(T)$ of the second-order axial displacements at the top of the cylinder, due to tension and torsion with the interface position r_1 for a soft bilayered composite.

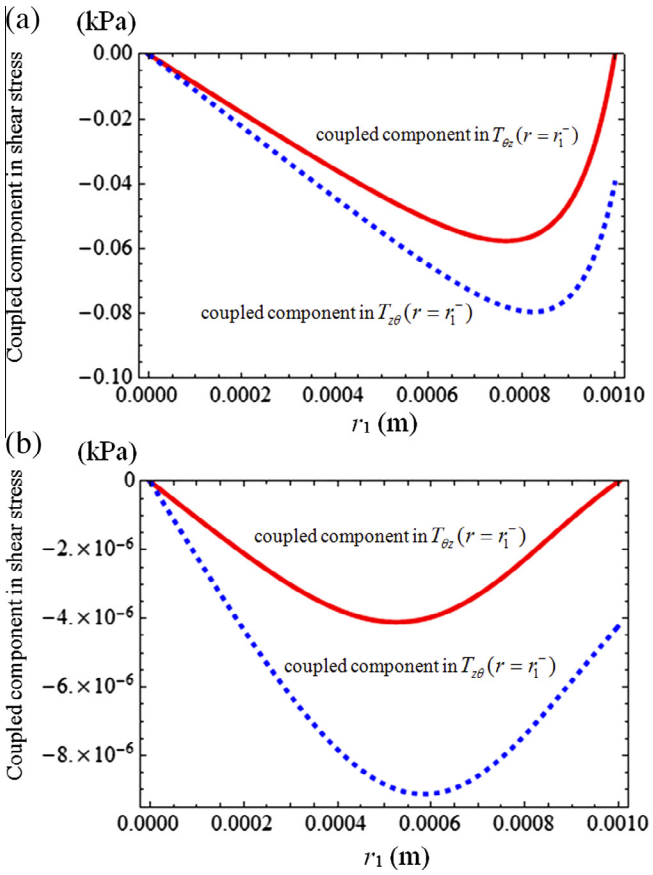

Fig. 9. Variation of the second-order coupled component in the shear stress $T_{\theta z}(r_1^-)$ (solid line) and $T_{z\theta}(r_1^-)$ (dashed line) with interface position r_1 for: (a) soft composite and (b) metallic composite.

in the transverse plane. However, it is possible to develop a transversely isotropic second- or even higher-order model, and the associated number of elastic constants can be reduced if the further assumption of incompressibility is built directly into the theory.

4. Further discussion

The Poynting effect has mostly been investigated for homogeneous materials. The results in this paper are relevant for composite materials under complex loading. They have many applications as discussed below.

First, many natural biomaterials are composites, architecturally hierarchical, and are often subjected to complex multiaxial loads in their physiological environment. Criscione et al. (1999) conducted finite extension and torsion experiments on papillary muscles in order to characterize their constitutive behavior. They modeled the material as a bi-layered composite consisting of a core of myocardium inside a thin sheath of endocardium. We determined the third-order elastic constants l, m and n for both the core and the sheath. Haberl et al. (2004) investigated experimentally the kinematic response of lumbar spinal units subjected to torsion, compression and flexion/extension. These units can be considered as a composite material with a soft material (nucleus pulposus) between them. Tóth et al. (2005) studied the mechanical parameters of arterial walls, specifically related to human brain aneurysm (bulge along a blood vessel). The authors modeled the arterial wall as a three-layer cylindrical composite subjected to combined extension, torsion and inflation (which mimic real physiological conditions).

Understanding of the mechanics of natural biomaterials in their operating environment is crucial to the development of artificial tissues and organs in the field of medicine. Tissue and organ damage or failure is a major health issue and there has been intensive research in the field (Persidis, 1999; Danoux et al., 2013). The results in this paper are relevant to the design of bio-mimicking composite polymers, natural and/or synthetic, for use as replacement tissues.

Soft biomaterials such as collagen, fibrin, vimentin, neurofilaments and actin demonstrate the Poynting effect, as pointed out by Janmey et al. (2007). In the movement of micrometer-sized mitochondria through the cytoskeleton of a narrow axon, the negative Poynting effect (which generates negative normal stress) may facilitate organelle motion without distending the axon diameter. The large stresses generated by the Poynting effect can caused significant effect on the overall force balance in the cytoskeleton under shear or torsion. Studies of the Poynting effect are therefore of key interest and form the main focus of our paper.

Second, the results may assist in the design of medical instruments. A key requirement in the development of high-fidelity surgical simulators is the realistic modeling of the interaction between surgical instruments and human organs. Human organs are generally inhomogeneous and multilayered. The Poynting effect can result in differences in force or displacement magnitude larger than the absolute human perception threshold for force or displacement discrimination in some tissues (e.g. myocardial tissues) but not in others (e.g. brain tissues), as described in Misra

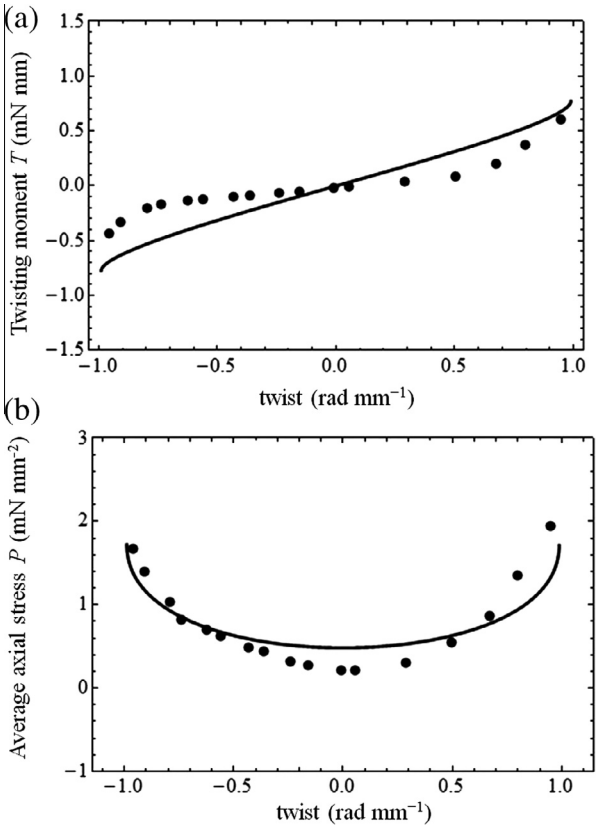

Fig. 10. Comparison of the theoretical predictions of (a) twisting moment T and (b) average axial stress P with the experimental data of Criscione et al. (1999) for cardiac papillary muscles.

et al. (2010). Using our results, the magnitude of the forces or displacements of multilayered human organs generated by the Poynting effect can be predicted.

Third, the Poynting effect can be utilized in the design and operation of actuators and sensors. A bio-inspired polymer composite actuator can be made, based on the phenomenon that an input torsion may generate a large output axial displacement, which can be used to actuate a connecting device. According to our results, materials parameters and interface positions can be used to adjust (and possibly maximize) the ratio of output displacements to input torsion. Similarly, a torsionally stressed actuator, if subjected to a further input axial force, may generate an additional output twist, according to the axial force–twist effect. The amount of twist can likewise be controlled by the material elasticity and the interface design. Conversely, a bio-inspired polymer sensor can be designed for sensing torsional moments based on the Poynting effect, i.e., measurements of the axial length change can be used to detect and indeed predict the magnitude of the torsional moment.

Furthermore, the results obtained also have important implications for the development of accurate torsion test protocols for the determination of material properties of soft tissues. If a linear or even a nonlinear model is used for analyzing a soft tissue in a combined torsion and extension experiment in which both the Poynting effect and axial force–twist effect are neglected, there could be significant errors in measuring both the shear modulus (due to the extra twisting caused by the axial force–twist effect) and the Young's modulus (due to the extra extension or contraction caused by the Poynting effect).

The celebrated Poynting effect, in which a cylindrical specimen extends under a torque, is a second-order effect that has been well-investigated for homogeneous materials. This paper develops expressions, i.e., Eqs. (2.42) and (2.37), which permit a prediction of the Poynting effect for both homogeneous and composite cylinders, respectively. Eq. (2.42) shows that the Poynting effect can be predicted by the four elastic constants λ, μ, m and n as well as T and R. Similarly, Eq. (2.37) requires the elastic constants λ_i, μ_i, m_i and n_i as well as T and r_i for a prediction. However, the elastic constants are lumped together as a single constant in the homogeneous case, while they are dispersed by r_i in the composite case. An examination of Eq. (2.37) reveals that, although it is nonlinear in λ_i, μ_i, it is strictly linear in m_i and n_i (no terms involving m_1m_2, m_1^2, etc.). These have some implications as elaborated below.

The Poynting effect decreases strongly with the cylinder radius ($1/R^6$) in the homogeneous case. The decrease is expected as it is more difficult to twist a thicker cylinder and the corresponding axial displacement would be smaller. The inverse sextic relation shows that the Poynting effect is two orders of magnitude smaller than the twist produced under torsion, which follows the inverse quartic law. The strong scale importance also suggests that the Poynting effect becomes much more significant at the micro- or nano-scale. This is in general also true for a composite cylinder but the interaction between the layer materials may result in anomalous behavior, e.g., an initial increase in the Poynting effect as the overall radius increases with the radius of the inner layer fixed. This is possible because the outer layer could have a stronger Poynting effect and increasing its size relative to the inner layer could lead to an initial increase in the effect.

Eq. (2.37) may be employed usefully in a reverse manner, i.e., determination of the elastic constants of the two layers, especially the third-order ones, by measuring the coefficient D of composites having various combinations of r_i. The interspersed nature of the elastic constants and the radii results in a system of algebraic equations nonlinear in the second-order constants and linear in the third-order constants. These equations can be solved for the unknown elastic constants. A simple illustration of this is the determination of the third-order constants m_i and n_i for the two layers, assuming that the second-order constants (the Lamé constants, or the usual Young's moduli and Poisson ratios) have been measured by other methods. By measuring the Poynting effect coefficients for four different combinations of r_i, a simple system of four linear algebraic equations where the four unknowns m_i and n_i can be solved easily. Provided that the Poynting effect is significant for the soft materials and amenable to measurements, and provided that composites can be fabricated from the constituent materials, this may offer an alternative method for the determination of third-order elastic constants, usually measured via acousto-elastic methods (Catheline et al., 2003; Destrade et al., 2010). We note that the second-order effects in composite cylinders under pure axial loading may be similarly used to estimate the elastic constants. The relevant parameters that appear in the radial and axial displacement expressions are combinations of λ_i, μ_i, m_i and n_i as well as P and r_i. Hence, both axial and torsional loadings of composite cylinders can be used in combination for the determination of second- and third-order elastic constants.

In the course of this work, it is also found that the axial force–twist effect, in which a cylindrical specimen, homogeneous or otherwise, twists under an axial loading in the presence of a torque, is also possible within the second-order theory. This second-order effect is an intrinsically coupled phenomenon, meaning that both the torque and axial loading must be present for it to materialize. This is unlike the Poynting effect, which appears even in the absence of axial loading. Its importance is highlighted in the paper, and its dependence on the elastic constants and the interface position of a composite cylinder is emphasized. Both the Poynting and axial force–twist effects, as well as other second-order effects, appear to be significant in soft materials but less so in metallic materials. Such findings could be useful for applications in regenerative

medicine and for the design of bio-inspired soft materials, e.g., through the selection of material inhomogeneity (elastic constants of layers) and geometrical inhomogeneity (layer thicknesses).

Although this work considers inhomogeneity and nonlinearity, it does not consider elastic anisotropy or time-dependent phenomena such as viscoelasticity. Analytical solutions in elastically anisotropic and geometrically regular composites are likely obtainable using higher-order elasticity theories. Also, generalization of the solutions for multilayered composites can be achieved without difficulty, as shown in this paper for bi-layered and homogeneous cylinders. The solutions of the differential equations of equilibrium are not complicated, but the constants in the solutions will contain complex combinations of the elastic and geometric parameters. However, this is acceptable because the constants in the differential equations can be evaluated numerically with ease before the equations are actually solved.

5. Conclusions

The second-order effects in homogeneous and bi-layered cylinders under pure torsion, pure axial loading and combined loading have been investigated in this paper within the framework of second-order elasticity. The major contributions and findings can be summarized as follows.

First, analytical solutions have been derived for both homogeneous and bi-layered cylinders under the various loading modes, starting consistently from the equilibrium equations for the first Piola–Kirchhoff stress.

Second, the second-order effects in the displacement and stress fields have been identified, and their dependence on the elastic constants and geometrical parameters has been studied in detail. The second-order elastic fields under combined loading cannot be obtained from a simple superposition of the fields under the respective pure loading modes.

Third, the mechanics of the Poynting effect of a composite has been investigated in some depth. Explicit Poynting effect coefficients are given for both homogeneous and bi-layered composites. The key findings include: an amplified Poynting effect is possible above that of homogeneous materials, depending on the interface position; the effect is also dependent on the material configuration within the composite; the dependence of the effect on the overall cylinder size obeys an inverse sextic law.

Fourth, the axial force–twist effect has been explored. This effect is second-order in nature and exists only under combined torsion and axial loading.

Finally, the analytical solutions obtained may be used as the theoretical basis for the experimental estimation of third-order elastic constants.

References

Alexopoulos, L.G., Haider, M.A., Vail, T.P., Guilak, F., 2003. Alterations in the mechanical properties of the human chondrocyte pericellular matrix with osteoarthritis. J. Biomech. Eng. 125, 323–333.

Beebe, D.J., Moore, J.S., Bauer, J.M., Yu, Q., Liu, R.H., Devadoss, C., Jo, B.H., 2000. Functional hydrogel structures for autonomous flow control inside microfluidic channels. Nat. Biotechnol. 404, 588–590.

Bhargava, R., Gupta, P.K., 1976. Second-order torsion problem of a homogeneous isotropic compressible multiply-connected elastic cylinder. Int. J. Non-Linear Mech. 11, 239–250.

Bhargava, R., Gupta, P.K., 1979. Second-order torsion problem of a cylinder consisting of different isotropic homogeneous compressible elastic materials. Int. J. Non-Linear Mech. 14, 23–33.

Blackburn, W., Green, A., 1957. Second-order torsion and bending of isotropic elastic cylinders. Proc. R. Soc. Lond. Ser. A, Math. Phys. Sci. 240, 408–422.

Boyce, B.L., Grazier, J.M., Jones, R.E., Nguyen, T.D., 2007. The mechanics of soft biological composites, Sandia Report, 122p.

Brazel, C.S., Peppas, N.A., 1999. Dimensionless analysis of swelling of hydrophilic glassy polymers with subsequent drug release from relaxing structures. Biomaterials 20, 721–732.

Browning, M., Dempsey, D., Guiza, V., Becerra, S., Rivera, J., Russell, B., Höök, M., Clubb, F., Miller, M., Fossum, T., 2012. Multilayer vascular grafts based on collagen-mimetic proteins. Acta Biomater. 8, 1010–1021.

Catheline, S., Gennisson, J.L., Fink, M., 2003. Measurement of elastic nonlinearity of soft solid with transient elastography. J. Acoust. Soc. Am. 114, 3087–3091.

Conti, E., Mackintosh, F.C., 2009. Cross-linked networks of stiff filaments exhibit negative normal stress. Phys. Rev. Lett. 102, 088102.

Criscione, J.C., Lorenzen-Schmidt, I., Humphrey, J.D., Hunter, W.C., 1999. Mechanical contribution of endocardium during finite extension and torsion experiments on papillary muscles. Ann. Biomed. Eng. 27, 123–130.

Cuchiara, M.P., Allen, A.C., Chen, T.M., Miller, J.S., West, J.L., 2010. Multilayer microfluidic PEGDA hydrogels. Biomaterials 31, 5491–5497.

Danoux, C., Tare, R., Smith, J., Bradley, M., Hunt, J.A., Oreffo, R.O.C., Habibovic, P., 2013. Development of materials for regenerative medicine: from clinical need to clinical application. In: de Boer, J., van Blitterswijk, C.A. (Eds.), Materiomics: High-Throughput Screening of Biomaterial Properties. Cambridge University Press, 206p (Chapter 9).

Destrade, M., Gilchrist, M.D., Ogden, R.W., 2010. Third- and fourth-order elasticities of biological soft tissues. J. Acoust. Soc. Am. 127, 2103–2106.

Detzel, C.J., Larkin, A.L., Rajagopalan, P., 2011. Polyelectrolyte multilayers in tissue engineering. Tissue Eng. Part B: Rev. 17, 101–113.

Diridollou, S., Patat, F., Gens, F., Vaillant, L., Black, D., Lagarde, J., Gall, Y., Berson, M., 2000. In vivo model of the mechanical properties of the human skin under suction. Skin Res. Technol. 6, 214–221.

Green, A.E., Shield, R., 1951. Finite extension and torsion of cylinders. Philos. Trans. R. Soc. Lond. Ser. A, Math. Phys. Sci. 244, 47–86.

Haberl, H., Cripton, P.A., Orr, T.E., Beutler, T., Frei, H., Lanksch, W.R., Nolte, L.P., 2004. Kinematic response of lumbar functional spinal units to axial torsion with and without superimposed compression and flexion/extension. Eur. Spine J. 13, 560–566.

Han, I.S., Han, M.H., Kim, J., Lew, S., Lee, Y.J., Horkay, F., Magda, J.J., 2002. Constant-volume hydrogel osmometer: a new device concept for miniature biosensors. Biomacromolecules 3, 1271–1275.

Hiki, Y., Granato, A.V., 1966. Anharmonicity in noble metals; higher order elastic constants. Phys. Rev. 144, 411–419.

Hirth, J.P., Lothe, J., 1982. Theory of Dislocations. Krieger Publishing Company.

Horgan, C.O., Murphy, J.G., 2011. Torsion of incompressible fiber-reinforced nonlinearly elastic circular cylinders. J. Elast. 103, 235–246.

Hughes, D.S., Kelly, J.L., 1953. Second-order elastic deformation of solids. Phys. Rev. 92, 1145–1149.

Janmey, P.A., Mccormick, M.E., Rammensee, S., Leight, J.L., Georges, P.C., Mackintosh, F.C., 2007. Negative normal stress in semiflexible biopolymer gels. Nat. Mater. 6, 48–51.

Jessel, N., Oulad-Abdelghani, M., Meyer, F., Lavalle, P., Haikel, Y., Schaaf, P., Voegel, J.-C., 2006. Multiple and time-scheduled in situ DNA delivery mediated by β-cyclodextrin embedded in a polyelectrolyte multilayer. Proc. Natl. Acad. Sci. 103, 8618–8621.

Kang, H., Wen, Q., Janmey, P.A., Tang, J.X., Conti, E., MacKintosh, F.C., 2009. Nonlinear elasticity of stiff filament networks: strain stiffening, negative normal stress, and filament alignment in fibrin gels. J. Phys. Chem. B 113, 3799–3805.

Kirchhof, K., Hristova, K., Krasteva, N., Altankov, G., Groth, T., 2009. Multilayer coatings on biomaterials for control of MG-63 osteoblast adhesion and growth. J. Mater. Sci. Mater. Med. 20, 897–907.

Kong, L., Ao, Q., Wang, A., Gong, K., Wang, X., Lu, G., Gong, Y., Zhao, N., Zhang, X., 2007. Preparation and characterization of a multilayer biomimetic scaffold for bone tissue engineering. J. Biomater. Appl. 22, 223–239.

Limbert, G., Taylor, M., 2002. On the constitutive modeling of biological soft connective tissues – a general theoretical framework and explicit forms of the tensors of elasticity for strongly anisotropic continuum fiber-reinforced composites at finite strain. Int. J. Solids Struct. 39, 2343–2358.

Mihai, L.A., Goriely, A., 2011. Positive or negative Poynting effect? The role of adscititious inequalities in hyperelastic materials. Proc. R. Soc. A – Math. Phys. 467, 3633–3646.

Mihai, L.A., Goriely, A., 2013. Numerical simulation of shear and the Poynting effects by the finite element method: an application of the generalised empirical inequalities in non-linear elasticity. Int. J. Non-Linear Mech. 49, 1–14.

Misra, S., Ramesh, K.T., Okamura, A.M., 2010. Modelling of non-linear elastic tissues for surgical simulation. Comput. Method Biomech. 13, 811–818.

Murnaghan, F.D., 1951. Finite Deformation of an Elastic Solid. John Wiley, New York.

Persidis, A., 1999. Tissue engineering. Nat. Biotechnol. 17, 508–510.

Powell, B.E., Skove, M.J., 1982. A combination of 3rd-order elastic-constants of aluminum. J. Appl. Phys. 53, 764–765.

Poynting, J.H., 1909. On pressure perpendicular to the shear planes in finite pure shears, and on the lengthening of loaded wires when twisted. Proc. R. Soc. Lond. A – Cont A 82, 546–559.

Rivlin, R.S., 1953. The solution of problems in second-order elasticity theory. Arch. Rat. Mech. Anal. 2, 53–81.

Sindhu, S., Menon, C.S., 2001. Third-order elastic constants and low-temperature lattice thermal expansion of the high-temperature structural material TiAl (vol. 34, p. 465, 2001). J. Phys. D Appl. Phys. 34, 1436.

Sofer, M., Rowe, E., Forder, D.M., Denstedt, J.D., 2002. Ureteral segmental replacement using multilayer porcine small-intestinal submucosa. J. Endourol. 16, 27–31.

Stammen, J.A., Williams, S., Ku, D.N., Guldberg, R.E., 2001. Mechanical properties of a novel PVA hydrogel in shear and unconfined compression. Biomaterials 22, 799–806.

Stella, J.A., Sacks, M.S., 2007. On the biaxial mechanical properties of the layers of the aortic valve leaflet. J. Biomech. Eng. 129, 757–766.
Tóth, B.K., Raffai, G., Bojtar, I., 2005. Analysis of the mechanical parameters of human brain aneurysm. Acta Bioeng. Biomech. 7, 3.
Volokh, K.Y., 2006. Lagrangian equilibrium equations in cylindrical and spherical coordinates. CMC – Comput. Mater. Con. 3, 37–42.
Wang, D., Wu, M.S., 2013a. Stress and displacement fields in soft cylindrical multilayers. Int. J. Solids Struct. 50, 511–518.
Wang, D., Wu, M.S., 2013b. Second-order elasticity of soft multilayer capsules: universal relations and parametric studies. Int. J. Eng. Sci. 73, 17–32.
Wu, M.S., Kirchner, H.O.K., 2010. Nonlinear elasticity modeling of biogels. J. Mech. Phys. Solids 58, 300–310.
Zhao, R., Sider, K.L., Simmons, C.A., 2011. Measurement of layer-specific mechanical properties in multilayered biomaterials by micropipette aspiration. Acta Biomater. 7, 1220–1227.
Zhu, H., Ji, J., Shen, J., 2004. Construction of multilayer coating onto poly-(dl-lactide) to promote cytocompatibility. Biomaterials 25, 109–117.
Zubov, L.M., 2001. Direct and inverse poynting effects in elastic cylinders. Dokl. Phys. 46, 675–677.